

This is the accepted manuscript made available via CHORUS. The article has been published as:

Correlated math

$$\text{angular distributions from the math}$$

$$\text{reaction for incident neutron energies from 6.5 MeV to 16.5 MeV}$$

K. J. Kelly, M. Devlin, J. M. O'Donnell, and E. A. Bennett

Phys. Rev. C **104**, 064614 — Published 23 December 2021

DOI: [10.1103/PhysRevC.104.064614](https://doi.org/10.1103/PhysRevC.104.064614)

Correlated n - γ Angular Distributions from the $Q = 4.4398$ MeV $^{12}\text{C}(n,n'\gamma)$ Reaction for Incident Neutron Energies from 6.5–16.5 MeV

K. J. Kelly^{1a}, M. Devlin¹, J. M. O'Donnell¹, and E. A. Bennett¹

¹*Los Alamos National Laboratory, Los Alamos, NM 87545, USA*

(Dated: November 23, 2021)

Neutron scattering cross sections and angular distributions represent one of the most glaring sources of uncertainty in calculations of nuclear systems. Even simple nuclei like ^{12}C show indications of errors in nuclear databases for scattering reactions. Measurements of inelastic neutron scattering have historically measured either the scattered neutrons or the nuclear de-excitation γ emission. Only a very small number of experiments attempted correlated measurements of both the neutron and γ data simultaneously, even though these n - γ correlations could be essential for understanding particle transport in nuclear systems. In this work we describe a measurement of the n , γ , and correlated n - γ angular distributions from the $Q=4.4398$ MeV $^{12}\text{C}(n,n'\gamma)$ reaction in a single experiment using an EJ-309 liquid scintillator detector array with wide angular coverage, and with a continuous incident neutron energy range from 6.5–16.5 MeV. We also provide a thorough covariance description of these results, including normalization of the probability distribution. While the measured n distributions agree well with the relatively large number of available literature measurements, there are comparatively very few measurements of the γ distributions from this reaction. However, our data support the presence of a non-zero a_4 Legendre polynomial component of the γ angular distribution suggested in past measurements, which is currently not incorporated in the ENDF/B-VIII.0 library despite the use of these same literature data for evaluation of the $^{12}\text{C}(n,n'\gamma)$ cross section. The correlated n - γ distribution measurements are limited to three measurements at incident neutron energies near 14 MeV. Our results do not generally agree with any of these literature measurements. We observe clear indications of significant changes in the n distribution for specific γ -detection angles and vice versa especially near thresholds for other reaction channels, which shows the potential for significant bias in experiments that, for example, tag on inelastic scattering using a single or small number of γ -detection angles and could impact particle transport calculations.

^a Corresponding Author

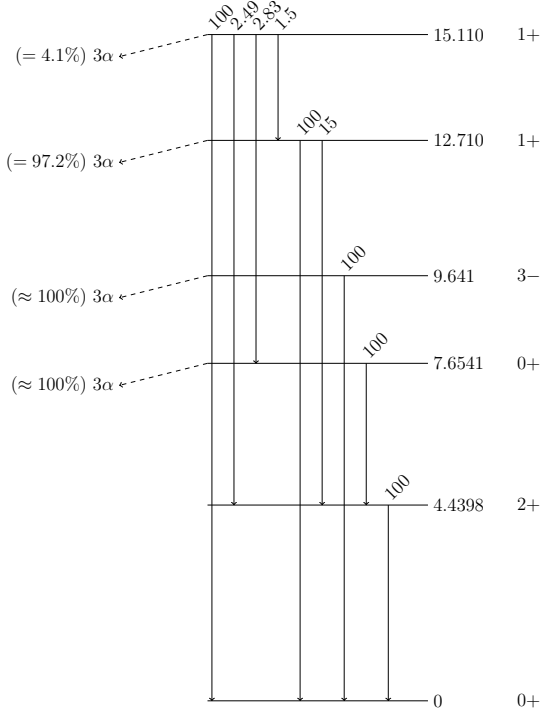


FIG. 1: A level diagram of ^{12}C is shown here. Level energies, γ intensities, and 3α breakup branching ratios are from Ref. [12]. Note that the γ intensities are relative within any given γ decay, and do not describe the relative split between γ and other decay modes. The percentage near to the 3α branches are branching ratios relative to γ decay. While all of the levels shown here are potentially populated within the incident energy range employed here, only excitations of the 4.4398 MeV state are reported in this work, isolated utilizing neutron kinematics. See the text for more details.

I. INTRODUCTION

Despite literature measurements going back nearly a century, neutron scattering cross sections and angular distributions are still one of the most significant sources of uncertainty in simulations of nuclear systems [1, 2]. Actinide scattering cross sections are particularly poorly known because of the high level densities and presence of fission, ($n,2n$), and other neutron-producing reactions, but even well-studied nuclei like ^{12}C show signs of nuclear data evaluation issues. A particular aspect of neutron scattering that has very few measurements on any nucleus is the correlated $n-\gamma$ emission from inelastic scattering. The details of these correlated distributions could be influential for particle and energy flow in these systems, and could also influence the interpretation of data obtained from measurements in which, for example, neutrons are measured in coincidence with a small number of selected γ -detection angles used as a “tag” on a desired reaction as in Refs. [3–5]. The assumption in these kinds of experiments is generally that the angular distribution of the tagging particle is independent of, e.g., the neutron-detection angle, though this is not necessarily guaranteed. Finally, while it is possible to calculate predictions of the correlated $n-\gamma$ distributions [6, 7], these details are not commonly explored and are also not included in Monte Carlo simulation tools, such as MCNP® [8].

Only three measurements of these kinds of data are known to the authors, and they are limited to incident neutron energies of approximately 14–15 MeV with very limited coverage of the total phase space [9–11]. State-of-the-art neutron scattering theories also are only able to predict these two-dimensional distributions for specific cases and can not describe the complicated interactions between various excited states of a given nucleus, thus experimental data on these correlations are of vital importance.

In this work we report on a measurement of the correlated $n-\gamma$ angular distribution from inelastic neutron scattering on ^{12}C with the residual in the first excited state at 4.4398 MeV (i.e., the $Q = 4.4398 \text{ MeV } ^{12}\text{C}(n,n'\gamma)$ reaction) for continuous incident neutron energies from $E_n^{inc} = 6.5\text{--}16.5 \text{ MeV}$ at the Los Alamos Neutron Science Center (LANSCE). The level structure of ^{12}C is shown in Fig. 1 for reference [12]. With the exception of the state at 15.110 MeV, ^{12}C excitations above the 4.4398 MeV state typically undergo 3α decay either by a sequential two-body reaction or a

three-body breakup process [13, 14]. The measurements described in this work utilized pulse shape discrimination (PSD) techniques to separately analyze the neutron and γ data. The experimental setup is described in Sec. II. The data analysis procedures for separating n and γ data, measurement of random-coincidence backgrounds, application of in-target multiple scattering corrections, neutron detector response treatment, and extraction of the normalized angular distributions n - γ angular distributions with the associated covariance are described in Secs. III A – III E. Finally, results are shown in Sec. IV, with concluding remarks given in Sec. V.

II. EXPERIMENTAL SETUP

The relevant details of the experimental area are described here. The reader is referred to Refs. [15–17] for more detail. The white neutron source at the Weapons Neutron Research (WNR) facility at LANSCE originates from an 800 MeV proton beam incident on a tungsten spallation target. The proton beam is structured into “micropulses” and “macropulses.” Each proton micropulse is a 150 ps wide pulse of protons, separated by approximately 1.8 μ s from any neighboring micropulse. Each macropulse consists of approximately 347 micropulses, and WNR received an average of 100 macropulses per second during this experiment. A signal, referred to as the t_0 signal, was provided to the experimental area indicating that a new proton micropulse was impinging on the spallation target. The measurements described in this work were carried out at WNR flight path 15L, located 21.5 m from the spallation target and 15° to the left of the incident proton beam axis. This particular flight path is specially designed for neutron detection measurements; there is a 2 m “get-lost basement” beneath the target area and all shielding walls are over 2 m from the target, thus neutron scattering backgrounds are significantly reduced compared to other experimental environments [15, 18]. The target for this experiment was a cylindrical graphite piece of approximately 1 in diameter and 2.5 in long.

All data were measured with a fifty-four detector EJ-309 [19] liquid scintillator detector array, each with an R4144 Hamamatsu PMT attached [20]. These detectors span nine evenly-spaced angles in θ (polar angle) from 30–150° with respect to the beam direction, with six detectors per θ at ϕ (azimuthal) angles of ±24, 57, and 90° with respect to vertical. High voltages were supplied by a CAEN SY4527 HV supply [21]. Both the t_0 signals and all liquid scintillator signals asynchronously triggered data on individual channels of a series of CAEN 1730B waveform digitizers [22] and recorded using the MIDAS data acquisition framework [23]. Typical data rates for this experiment were approximately 7.5 MB/s yielding measured count rates of approximately 2000 counts per second before cuts on signal integral for both neutron and γ -ray detections, and data “runs” were limited 10 minutes each. Coincidences were assembled offline as described in the following section.

III. DATA ANALYSIS

The important data analysis steps are described in this section. The offline formation of n - γ coincidences and random-coincidence backgrounds are described in Secs. III A and III B, both of which were handled using only the experimental data with the target in place. In-target multiple scattering corrections and neutron detector response treatments were handled using Monte Carlo N-Particle (MCNP® [8]) simulations and are described in Secs. III C and III D. The final calculations of the normalized n , γ , and correlated n - γ angular distributions with the associated covariances are described in Sec. III E.

A. Offline Formation of Coincidences

Neutron and γ signals were separated based on the PSD ratio of the pulse tail integral to the full pulse integral. These integration windows were defined to be 200 and 270 ns long, respectively. Integration windows were set in software and applied via the CAEN digitizers utilized for this experiment. Signal integrals were calculated from the data as they were collected. Values of the PSD parameter for these data were calculated in post-processing analysis. The PSD spectrum obtained for this experiment is shown in Fig. 2 with the corresponding n and γ gates. Each detector was characterized as both a neutron and a γ detector in analysis, with signals passing either PSD gate separated and treated accordingly in the subsequent analysis steps. While γ signals were selected using a relatively tight PSD gate that did not go too low in pulse integral in order to avoid overlap with neutrons. This cutoff for the γ -ray integrals at approximately 0.007 V μ s does not reduce the detection efficiency for γ rays from the desired reaction and only serves to remove background from the data because the cutoff is far below the primary and escape peaks of the 4.44 MeV γ ray of interest. The neutron PSD gate was opened more broadly with an additional selection on neutrons via the kinematic gate shown in Fig. 3, showing data from the $^{12}\text{C}(n,n'\gamma)$ measurement described in this

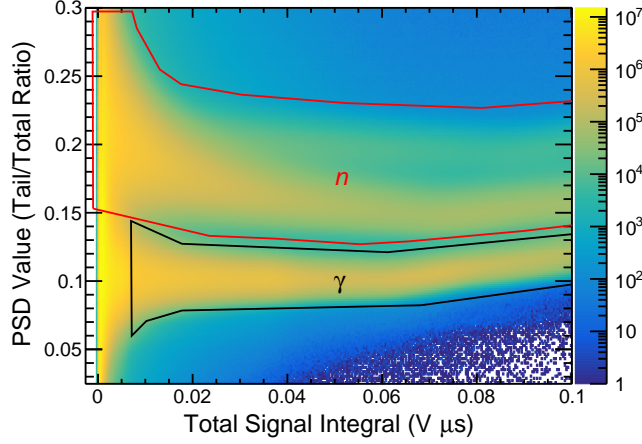


FIG. 2: (color online) The measured PSD spectrum is shown here. The n and γ counts are labelled with their corresponding gates shown in red and black, respectively.

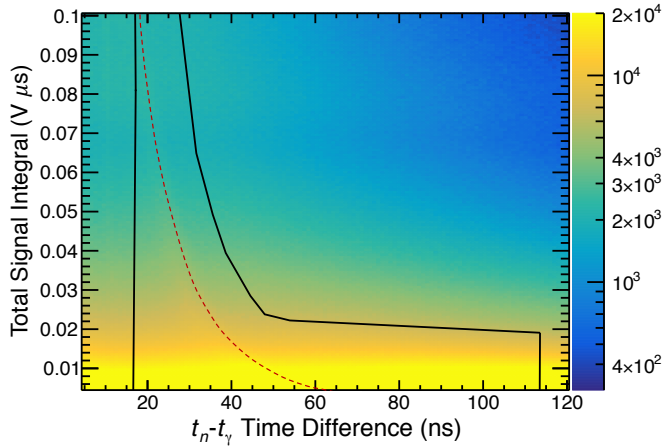


FIG. 3: (color online) The kinematic spectrum from the $^{12}\text{C}(n,n'\gamma)$ measurement is shown here with the kinematic gate required to select the desired neutrons shown in black is shown here with the approximate trend of the peak of the signal integral versus measured neutron time of flight is shown as the red dashed line.

work. The n kinematic band is only just visible above the pervasive backgrounds in Fig. 3, and thus the limits of the kinematic gate were determined by measurements of prompt fission neutrons from the spontaneous fission of ^{252}Cf in a separate experiment using an intermediate fission tag instead of an intermediate γ ray for outgoing neutron energy measurements. The use of ^{252}Cf spontaneous fission is well-suited for guidance of the $^{12}\text{C}(n,n')$ data analysis because both measurements produce neutron spectra that span a similar wide range in outgoing neutron energy. Note that this produces no dependence of the results presented in this work on ^{252}Cf as the leading relation of the neutron signal integral to measured time of flight, i.e., the placement of the neutron kinematic gate, is not sensitive to differences between the ^{252}Cf and carbon scattering experimental setups. Detection times t_n and t_γ were recorded for each n and γ detection, with the t_γ values corrected for the γ transit time from the target to the detector so that they could be used as a measure of the $^{12}\text{C}(n,n'\gamma)$ reaction time.

Signals were assembled into coincident $\{t_0, t_n\}$ and $\{t_0, t_\gamma\}$ pairs offline, and these were subsequently assembled into “double coincidences” of t_n and t_γ times with a common t_0 signal, denoted $\{t_\gamma, t_n; t_0\}$. Incident neutron energies were calculated using the $t_\gamma - t_0$ time difference, and outgoing neutron energies were calculated using the $t_n - t_\gamma$ time difference. These energies were then plotted on a two-dimensional histogram of outgoing versus incident neutron energy, as shown in Fig. 4(a). The intermediate γ detection acts as a tag for inelastic neutron scattering, and thus we primarily expect a neutron kinematic band corresponding to the $Q = 4.4398 \text{ MeV } ^{12}\text{C}(n,n'\gamma)$ reaction from the tag on the corresponding $\sim 4.4 \text{ MeV } \gamma$. The band extending from $(E_n^{inc}, E_n^{out}) \approx (5.3 \text{ MeV}, 0.5 \text{ MeV}) - (15 \text{ MeV}, 10 \text{ MeV})$

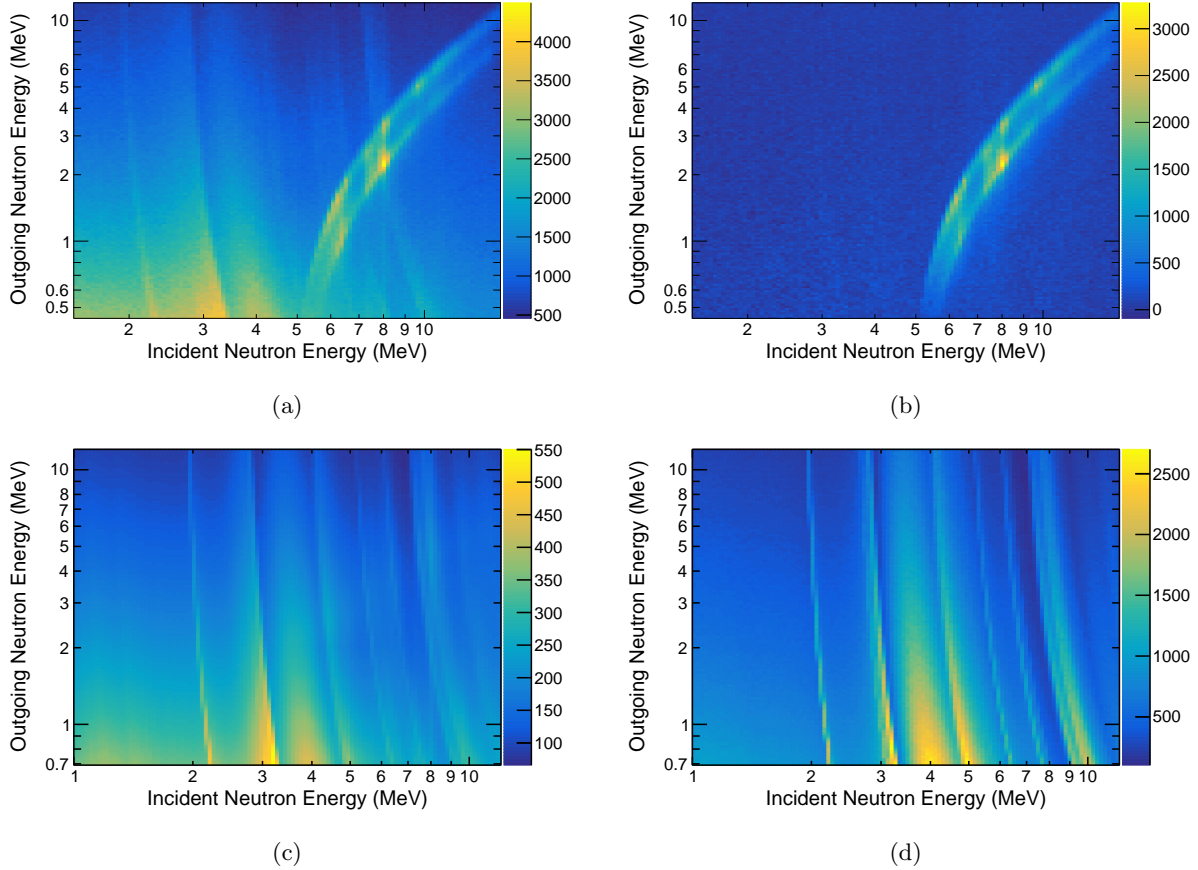


FIG. 4: (color online) Shown here are (a) the measured data in the form of a two-dimensional E_n^{out} vs. E_n^{inc} spectrum for carbon neutron scattering with an intermediate γ tag integrated over all angles, (b) the background-subtracted data spectrum integrated over all angles, (c) the measured background for a neutron-detection angle of 30° , and (d) a calculation of the expected background from the $^{12}\text{C}(n,n)$ elastic scattering reaction for a neutron-detection angle of 30° assuming a random γ ray uniformly-distributed in time and no neutron scattering effects. See the text for a discussion.

in Fig. 4(a) fits the expected trend, though there are clearly large backgrounds beneath this band. The structures present in these backgrounds will be discussed in the next section. The total counts in the kinematic band for each n - and γ -detection angle were calculated by gating *on the peak* of this kinematic band after background subtraction.

B. Random-Coincidence Backgrounds

Backgrounds from reactions on other nuclei should be minimal given the ease with which pure carbon targets can be produced, and so backgrounds from n and γ signals randomly in coincidence form the more problematic backgrounds. These random-coincidence backgrounds under the true double coincidence detections from the reaction of interest were calculated using the method of Ref. [24]. Applications of this method for neutron detection with an intermediate fission trigger have been described in Refs. [15] and [17], and so only a brief description will be given here. Provided that the detection rate of uncorrelated (random) $\{t_0, t_n\}$ and $\{t_0, t_\gamma\}$ pairs is much higher than the correlated (true) $\{t_\gamma, t_n; t_0\}$ double coincidence rate and the individual detector count rates are small compared to the inverse of the coincidence spectrum bin width ($\Delta_t = 0.25$ ns), the Poisson distributed $\{t_0, t_n\}$ and $\{t_0, t_\gamma\}$ rates before double coincidence formation can be used to calculate the rate of random double coincidences, r_c , as

$$r_c = r_n r_\gamma \Delta_t, \quad (1)$$

where r_n and r_γ denote the $\{t_0, t_n\}$ and $\{t_0, t_\gamma\}$ rates respectively.

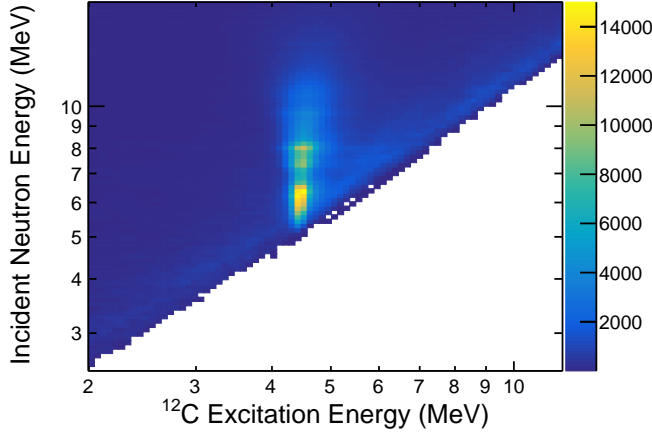


FIG. 5: (color online) A missing mass representation of the observed counts is shown here. The vertical line of counts at an excitation energy of 4.44 MeV is clearly seen.

This background was calculated as a function of E_n^{inc} and E_n^{out} , and was subtracted from the data in Fig. 4(a) to produce the data shown in Fig. 4(b). The measured background spectrum for an outgoing neutron detection angle of 30° is shown in Fig. 4(c). The dominant structures present in this background spectrum are quite pronounced, and don't appear to follow typical kinematic trends, i.e., the measured E_n^{out} seems to decrease with increasing E_n^{inc} . The structures in the measured background spectra can be understood by considering neutrons emitted from reactions that do not emit coincident γ rays, with the $^{12}\text{C}(n,n)$ elastic scattering reaction being the most likely in this case. If a γ ray is randomly detected within the coincidence window relative to the t_0 and t_n times, then E_n^{inc} and E_n^{out} values will be calculated using the intermediate t_γ time. There does exist a true reaction time for the elastic scattering reaction here from which the correct E_n^{inc} and E_n^{out} values could be calculated, but there is no measurement of this reaction time and the measured random t_γ likely does not correspond to this reaction time. If t_γ is before the true reaction time, the incident neutron time of flight is measured to be too short and the outgoing neutron time of flight too long, leading to calculated E_n^{inc} and E_n^{out} values that are too high and too low, respectively. Conversely, if this random t_γ time occurs after the true reaction time, E_n^{inc} and E_n^{out} values that are too low and too high, respectively, are measured instead. This appears to be the source of the structures in the measured backgrounds.

To demonstrate this suggested source of random-coincidence backgrounds in the measured data, the ENDF/B-VIII.0 [2] $^{12}\text{C}(n,n)$ elastic scattering differential cross section at an outgoing neutron detection angle of 30° in the laboratory frame was used as input for a calculation of the expected background trends. The elastic scattering cross section is roughly a factor of $\sim 5\text{--}10$ higher than the inelastic cross section on average, depending on incident neutron energy, and so elastically scattered neutrons are a likely source for neutrons in measured to be accidentally in coincidence. A nominal incident neutron flux spectrum for the employed experimental flight was randomly sampled, and the expected outgoing neutron energies were calculated for each sample of the incident flux assuming relativistic kinematics for the $^{12}\text{C}(n,n)$ reaction. These energies were converted to time of flight, and then were shifted according to an intermediate t_γ relative to the true elastic scattering reaction time sampled randomly and uniformly in time. Altered energies were calculated from these shifted times of flight. Counts in an identical histogram as in Fig. 4(c) were then assigned based on the evaluation cross section. This calculation yielded the spectrum in Fig. 4(d), which is to be compared with the spectrum in Fig. 4(c). The dominant structures appear to be nearly identical in shape and position, supporting this as the suggested primary source of random-coincidence backgrounds here. The agreement between Figs. 4(c) and 4(d) is not exact because the calculation used to generate Fig. 4(d) does not include any neutron scattering effects, and because the source, energy distribution, time distribution, relative intensity at each detector, and other properties of these random γ rays are not well known. Thus, the assumption of an intermediate t_γ sampled uniformly in time and with equal probability for detection (i.e., γ -detection efficiency) within coincidence windows for each incident neutron energy is almost certainly incorrect. There are also more contributing reactions to the random-coincidence backgrounds than elastic scattering alone. Nevertheless, the clear similarities between Figs. 4(c) and 4(d) suggest that elastic scattering is the primary contribution to the random-coincidence background.

After subtraction of these backgrounds to obtain the spectrum in Fig. 4(b), effectively all of the background counts beneath the $^{12}\text{C}(n,n'\gamma)$ data have been removed. The splitting of this single reaction band based on the kinematics involved with n detections at different detection angles is now evident in Fig. 4(b) as well. The data in Fig. 4(b) are alternatively shown in terms of the missing mass from the measured reaction kinematics, which is trivially converted

to residual excitation energy as shown in Fig. 5 with the vertical line of counts at the expected excitation energy of 4.44 MeV clearly seen.

C. In-Target Multiple Scattering Corrections

Corrections for multiple scattering were obtained using MCNP®6 [8] with the PTRAC output format [25]. Incident neutrons were set to impinge on a target of identical size and position as in the experimental configuration. The experimental environment outside of the target relied on the extensive and well-studied simulation of WNR flight path 15L with the employed liquid scintillator array. This simulation has been described many times in previous works [15–17, 26], and thus only minor modifications were needed to reproduce the environment for the experiment described in this work. The PTRAC output format allowed for the $Q = 4.4398 \text{ MeV } ^{12}\text{C}(n,n'\gamma)$ reaction to be perfectly separated from elastic scattering and other reactions occurring within the target, and n detections from this reaction were separated according to the number of interactions that occurred within the target before detection. The in-target multiple scattering correction factors, $\psi_{n,\alpha}(\theta_n)$, were calculated separately for each neutron detection angle, θ_n and for a given incident neutron energy. The index α is used to denote unique incident neutron energies, $E_n^{inc} = E_\alpha$. These correction factors are calculated via the ratio of counts with only a single target interaction, $s_\alpha(\theta_n)$, to the sum of counts with single and multiple in-target reactions, $m_\alpha(\theta_n)$, i.e.,

$$\psi_{n,\alpha}(\theta_n) = \frac{s_{n,\alpha}(\theta_n)}{s_{n,\alpha}(\theta_n) + m_{n,\alpha}(\theta_n)}. \quad (2)$$

This correction was always <2%.

It should be noted that this correction implicitly assumes that the nuclear data library in the MCNP®6 simulation (ENDF/B-VIII.0 [2] in this case) is accurate. In reality, there may be inaccuracies in these cross sections or their associated angular distributions, and this may induce a systematic error in the in-target multiple scattering corrections applied here. The assessment of this systematic error is outside of the scope of this work, but this effect is expected to be small as the reliance on the ENDF/B-VIII.0 nuclear data is a perturbation on a <2% correction. A complete analysis of the scattering cross section and the $n\gamma$ distributions likely requires a forward-analysis approach in which the cross section and angular distribution included in the employed nuclear data library are varied to obtain agreement with the measured data.

D. Detector Response Treatment

Given that there is only a single γ emitted from the $Q = 4.4398 \text{ MeV } ^{12}\text{C}(n,n'\gamma)$ reaction regardless of the incident neutron energy and that the same total solid angle is covered for each polar detection angle, θ_γ , the γ efficiency, $\epsilon_\gamma(E_\gamma)$, for this experiment was treated as a constant. The doppler correction of this γ energy yielded a negligible effect as well. The environmental detector response of neutrons, on the other hand, is generally more complicated than for γ detection. In particular, it is not generally correct to assign a single one-dimensional detection efficiency curve for neutron detection, especially for continuous neutron distributions [17, 26–34]. However, for this specific reaction where a clear kinematic band for the desired reaction can be detected and isolated from all other reactions at all detection angles without the concern of contamination from neutron downscattering processes from higher-energy neutrons, a one-dimensional efficiency curve can be applied.

We have used the highly-detailed MCNP® simulation of the experimental environment described in Sec. III C to calculate the neutron detection efficiency curves for this work. A separate efficiency curve was calculated for each outgoing neutron angle, θ_n , because small details of the environment at each angle like, for example, the proximity to the nearest neighboring detector, can impact the inferred efficiency. Furthermore, since we are reporting only angular distributions in this work, corrections for neutron detection efficiency enter only as a ratio, $\rho_{n,\alpha}(\theta_n)$, of the efficiency for detecting neutrons of the energy observed at each θ_n to an arbitrary reference angle, chosen here to be the minimum θ_n of 30°. The difference in the observed outgoing neutron energy in the laboratory frame between the maximum and minimum detection angles is kinematically defined, and can range from 0.5 MeV at $E_\alpha = 6.5 \text{ MeV}$ to approximately 3.0 MeV at $E_\alpha = 16.5 \text{ MeV}$. This correction ranged from as little as 1.7% to as high as 30% between the minimum and maximum detection angles, depending on the incident neutron energy. The angle-integrated efficiency curve is shown in Fig. 6.

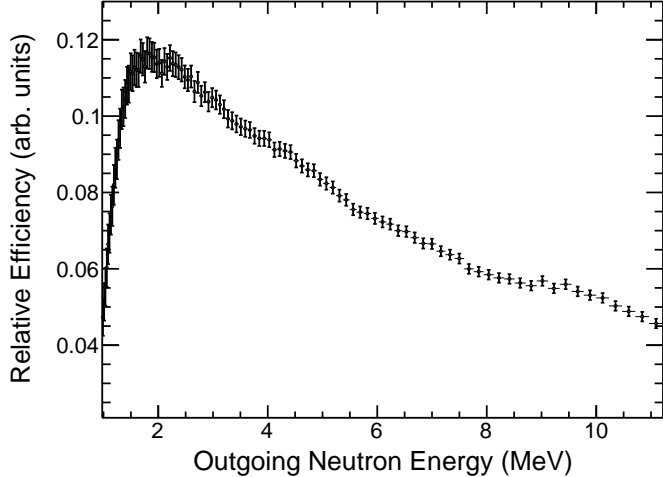


FIG. 6: The angle-integrated neutron detection efficiency curve shape is shown here. Uncertainties shown are statistical only.

E. Calculation of the Normalized Angular Distributions

The unnormalized n - γ angular distribution value at each incident neutron energy, E_α , each n -detection angle, θ_n , and each γ -detection angle, θ_γ , is denoted as $u_\alpha(\theta_n, \theta_\gamma)$ here and can be calculated as

$$u_\alpha(\theta_n, \theta_\gamma) = \frac{d_\alpha(\theta_n, \theta_\gamma) - b_\alpha(\theta_n, \theta_\gamma)}{\epsilon_\gamma(E_\gamma)\rho_{n,\alpha}(\theta_n)} \psi_{n,\alpha}(\theta_n), \quad (3)$$

where $d_\alpha(\theta_n, \theta_\gamma)$ and $b_\alpha(\theta_n, \theta_\gamma)$ are the data and background counts at E_α , θ_n , and θ_γ , and the remaining variables have been defined in the previous sections. Given this description of each measured angular distribution value, we will describe the methods for calculating the normalized n , γ , and correlated n - γ distributions in Secs. III E 1, III E 2, and III E 3, respectively.

1. n Distributions

In order to obtain the n distribution, the values in Eq. (3) must be summed over the γ -detection angles to yield

$$\begin{aligned} u_{n,\alpha}(\theta_n) &= \sum_{i=1}^{\Theta} u_\alpha(\theta_n, \theta_{\gamma,i}) \sin \theta_{\gamma,i}, \\ &= \frac{\psi_{n,\alpha}(\theta_n)}{\epsilon_\gamma(E_\gamma)\rho_{n,\alpha}(\theta_n)} \\ &\quad \times \sum_{i=1}^{\Theta} [d_\alpha(\theta_n, \theta_{\gamma,i}) - b_\alpha(\theta_n, \theta_{\gamma,i})] \sin \theta_{\gamma,i}. \end{aligned} \quad (4)$$

Here, Θ is the number of different θ angles. It could be argued that a more appropriate procedure would be to first fit the γ distribution for each n -detection angle to a series of Legendre polynomials, and integrate that function instead summing over the values obtained at each discrete angle. We have opted against this procedure in this work because of the even and fairly extensive angular coverage of the employed detector array. In this way the results are also all self-contained in the data and do not rely on details of a complex fit function, which should help to simplify the interpretation of the results.

The covariance matrix of the $u_{n,\alpha}(\theta_n)$ distribution at incident neutron energy E_α can be generally written as

$$\begin{aligned} & \text{cov} [u_{n,\alpha}(\theta_n), u_{n,\alpha}(\phi_n)] \\ &= \sum_{p_\alpha(\eta_n, \eta_\gamma)} \sum_{q_\alpha(\omega_n, \omega_\gamma)} \left[\frac{\partial u_{n,\alpha}(\theta_n)}{\partial p_\alpha(\eta_n, \eta_\gamma)} \right] \left[\frac{\partial u_{n,\alpha}(\phi_n)}{\partial q_\alpha(\omega_n, \omega_\gamma)} \right] \\ & \quad \times \text{cov} [p_\alpha(\eta_n, \eta_\gamma), q_\alpha(\omega_n, \omega_\gamma)], \end{aligned} \quad (5)$$

where p and q are variables representing one of the quantities in Eq. (3) [i.e., $d_\alpha(\theta_n, \theta_\gamma)$, $b_\alpha(\theta_n, \theta_\gamma)$, $\epsilon_\gamma(E_\gamma)$, $\rho_{n,\alpha}(\theta_n)$, or $\psi_{n,\alpha}(\theta_n)$], and θ , ϕ , η , and ω are potentially unique polar-axis detection angles. If p or q does not depend on the n - or γ -detection angle, then the sum is only over the relevant angle [e.g., $\psi_{n,\alpha}(\theta_n)$ does not depend on θ_γ , thus there is no sum over γ -detection angle]. These derivatives can be calculated as

$$\frac{\partial u_{n,\alpha}(\theta_n)}{\partial d_\alpha(\eta_n, \eta_\gamma)} = \frac{u_\alpha(\theta_n, \eta_\gamma) \sin \eta_\gamma}{d_\alpha(\theta_n, \eta_\gamma) - b_\alpha(\theta_n, \eta_\gamma)} \delta(\theta_n, \eta_n), \quad (6)$$

$$\frac{\partial u_{n,\alpha}(\theta_n)}{\partial b_\alpha(\eta_n, \eta_\gamma)} = -\frac{u_\alpha(\theta_n, \eta_\gamma) \sin \eta_\gamma}{d_\alpha(\theta_n, \eta_\gamma) - b_\alpha(\theta_n, \eta_\gamma)} \delta(\theta_n, \eta_n), \quad (7)$$

$$\frac{\partial u_{n,\alpha}(\theta_n)}{\partial \rho_{n,\alpha}(\eta_n)} = -\frac{u_{n,\alpha}(\theta_n)}{\rho_{n,\alpha}(\theta_n)} \delta(\theta_n, \eta_n), \quad (8)$$

$$\frac{\partial u_{n,\alpha}(\theta_n)}{\partial \psi_{n,\alpha}(\eta_n)} = \frac{u_{n,\alpha}(\theta_n)}{\psi_{n,\alpha}(\theta_n)} \delta(\theta_n, \eta_n). \quad (9)$$

The $\delta(\theta_n, \eta_n)$ parameters are Kronecker delta functions. Thus, Eq. (5) yields

$$\begin{aligned} & \text{cov} [u_{n,\alpha}(\theta_n), u_{n,\alpha}(\phi_n)] \\ &= \sum_{i=1}^{\Theta} \left(\frac{\partial u_{n,\alpha}(\theta_n)}{\partial d_\alpha(\eta_n, \eta_{\gamma,i})} \right)^2 \text{var} [d_\alpha(\theta_n, \eta_{\gamma,i})] \delta(\theta_n, \phi_n) \\ & \quad + \sum_{i=1}^{\Theta} \left(\frac{\partial u_{n,\alpha}(\theta_n)}{\partial b_\alpha(\eta_n, \eta_{\gamma,i})} \right)^2 \text{var} [b_\alpha(\theta_n, \eta_{\gamma,i})] \delta(\theta_n, \phi_n) \\ & \quad + \left(\frac{\partial u_{n,\alpha}(\theta_n)}{\partial \rho_{n,\alpha}(\eta_n)} \right)^2 \text{var} [\rho_{n,\alpha}(\eta_n)] \delta(\theta_n, \phi_n) \\ & \quad + \left(\frac{\partial u_{n,\alpha}(\theta_n)}{\partial \psi_{n,\alpha}(\eta_n)} \right)^2 \text{var} [\psi_{n,\alpha}(\eta_n)] \delta(\theta_n, \phi_n). \end{aligned} \quad (10)$$

The $\delta(\theta_n, \phi_n)$ functions are reflective of the diagonal covariances of the parameters in Eq. (3), and they force the covariance in Eq. (10) to be diagonal as well. Note that we have ignored any uncertainty contributions from the γ -detection efficiency as described in Sec. III D. This will be addressed again at the end of this section.

In order to properly report these angular distributions, they must be normalized with the resulting covariance propagation [35, 36]. The area of the n distribution at each E_α incident neutron energy, $A_{n,\alpha}$, was calculated using a series of trapezoidal areas to obtain

$$\begin{aligned} A_{n,\alpha} = \Delta_\theta & \left[-\frac{1}{2} (u_{n,\alpha}(\theta_{n,1}) + u_{n,\alpha}(\theta_{n,\Theta})) \right. \\ & \left. + \sum_{i=1}^{\Theta} u_{n,\alpha}(\theta_{n,i}) \right], \end{aligned} \quad (11)$$

where Δ_θ is the angle difference between each n -detection angle, which is a constant 15° for the array employed here.

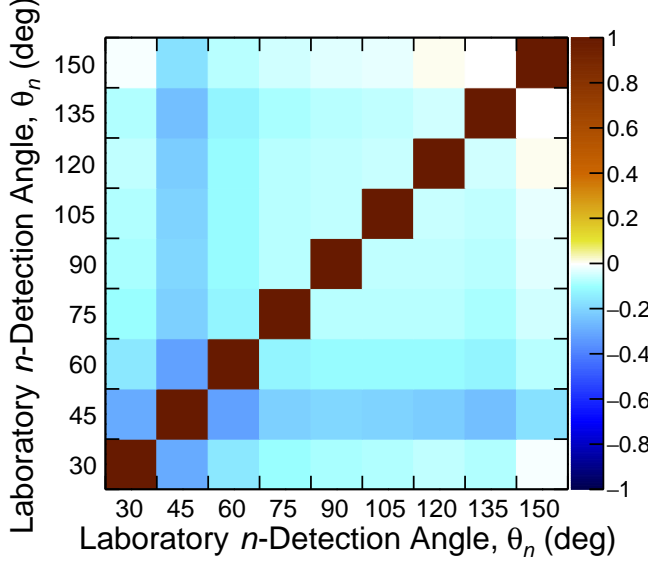


FIG. 7: (color online) An example normalized correlation matrix for the measured n distribution corresponding to $E_\alpha = 13.80\text{--}14.13$ MeV is shown here.

The normalized n distribution was calculated as

$$n_{n,\alpha}(\theta_n) = \frac{u_{n,\alpha}(\theta_n)}{A_{n,\alpha}}, \quad (12)$$

leading to a covariance described by

$$\text{cov} [n_{n,\alpha}(\theta_n), n_{n,\alpha}(\phi_n)] \quad (13)$$

$$= \sum_{i=1}^{\Theta} \sum_{j=1}^{\Theta} \left(\frac{\partial n_{n,\alpha}(\theta_n)}{\partial u_{n,\alpha}(\eta_{n,i})} \right) \left(\frac{\partial n_{n,\alpha}(\phi_n)}{\partial u_{n,\alpha}(\omega_{n,j})} \right)$$

$$\times \text{cov} [u_{n,\alpha}(\eta_n), u_{n,\alpha}(\omega_n)],$$

$$= \sum_{i=1}^{\Theta} \sum_{j=1}^{\Theta} \left(\frac{\delta(\theta_n, \eta_{n,i})}{A_{n,\alpha}} - \frac{u_{n,\alpha}(\eta_{n,i})}{A_{n,\alpha}^2} \frac{\partial A_{n,\alpha}}{\partial u_{n,\alpha}(\eta_{n,i})} \right)$$

$$\times \left(\frac{\delta(\phi_n, \omega_{n,i})}{A_{n,\alpha}} - \frac{u_{n,\alpha}(\omega_{n,i})}{A_{n,\alpha}^2} \frac{\partial A_{n,\alpha}}{\partial u_{n,\alpha}(\omega_{n,i})} \right)$$

$$\times \text{cov} [u_{n,\alpha}(\eta_n), u_{n,\alpha}(\omega_n)].$$

The $A_{n,\alpha}$ derivatives can be trivially calculated from Eq. (12). Note that while the covariance of the unnormalized distribution is diagonal in this case, the normalized covariance is not diagonal due to the dependence on the area of the unnormalized distribution. An example normalized correlation matrix corresponding to the n distribution for $E_\alpha = 13.80\text{--}14.13$ MeV is shown in Fig. 7.

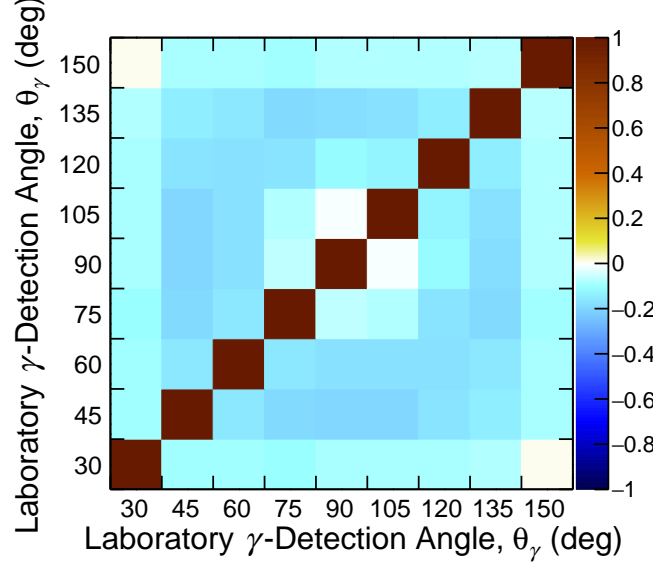


FIG. 8: (color online) An example normalized correlation matrix for the measured γ distribution corresponding to $E_\alpha = 13.80\text{--}14.13$ MeV is shown here.

2. γ Distributions

The unnormalized γ distributions follow a form that is similar to that of Eq. (4), namely

$$\begin{aligned} u_{\gamma,\alpha}(\theta_\gamma) &= \sum_{i=1}^{\Theta} u_\alpha(\theta_{n,i}, \theta_\gamma) \sin \theta_{n,i}, \\ &= \frac{1}{\epsilon_\gamma(E_\gamma)} \left[\sum_{i=1}^{\Theta} \frac{d_\alpha(\theta_{n,i}, \theta_\gamma) - b_\alpha(\theta_{n,i}, \theta_\gamma)}{\rho_{n,\alpha}(\theta_{n,i})} \right. \\ &\quad \times \left. \psi_{n,\alpha}(\theta_{n,i}) \sin \theta_{n,i} \right]. \end{aligned} \quad (15)$$

The primary difference between Eqs. (4) and (15) is that more parameters need to be summed over detection angles, which changes how the covariance of each parameter impacts the final result.

The covariance associated with this distribution becomes

$$\begin{aligned} \text{cov} [u_{\gamma,\alpha}(\theta_\gamma), u_{\gamma,\alpha}(\phi_\gamma)] &= \sum_{i=1}^{\Theta} \left(\frac{\partial u_{\gamma,\alpha}(\theta_\gamma)}{\partial d_\alpha(\eta_{n,i}, \eta_\gamma)} \right)^2 \text{var} [d_\alpha(\theta_{n,i}, \eta_\gamma)] \delta(\theta_\gamma, \phi_\gamma) \\ &\quad + \sum_{i=1}^{\Theta} \left(\frac{\partial u_{\gamma,\alpha}(\theta_\gamma)}{\partial b_\alpha(\eta_{n,i}, \eta_\gamma)} \right)^2 \text{var} [b_\alpha(\theta_{n,i}, \eta_\gamma)] \delta(\theta_\gamma, \phi_\gamma) \\ &\quad + \sum_{i=1}^{\Theta} \left(\frac{\partial u_{\gamma,\alpha}(\theta_\gamma)}{\partial \rho_{n,\alpha}(\eta_{n,i})} \right) \left(\frac{\partial u_{\gamma,\alpha}(\phi_\gamma)}{\partial \rho_{n,\alpha}(\eta_{n,i})} \right) \text{var} [\rho_{n,\alpha}(\eta_{n,i})] \\ &\quad + \sum_{i=1}^{\Theta} \left(\frac{\partial u_{\gamma,\alpha}(\theta_\gamma)}{\partial \psi_{n,\alpha}(\eta_{n,i})} \right) \left(\frac{\partial u_{\gamma,\alpha}(\phi_\gamma)}{\partial \psi_{n,\alpha}(\eta_{n,i})} \right) \text{var} [\psi_{n,\alpha}(\eta_{n,i})], \end{aligned} \quad (16)$$

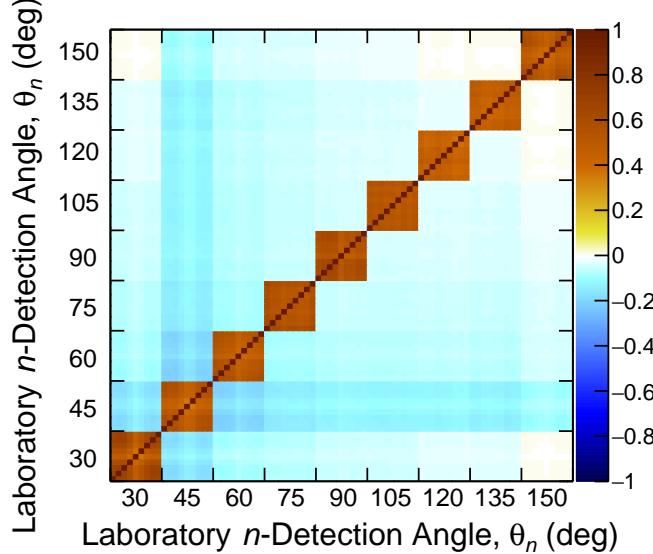


FIG. 9: (color online) An example normalized correlation matrix for the measured correlated n - γ distribution corresponding to $E_\alpha = 13.80\text{--}14.13$ MeV is shown here. Each θ_n bin on each axis contains each of the nine possible θ_γ angles. These θ_γ axis labels are not shown as they would be too small to display.

with the derivatives defined by

$$\frac{\partial u_{\gamma,\alpha}(\theta_\gamma)}{\partial d_\alpha(\eta_n, \eta_\gamma)} = \frac{u_\alpha(\eta_n, \theta_\gamma) \sin \eta_n}{d_\alpha(\eta_n, \theta_\gamma) - b_\alpha(\eta_n, \theta_\gamma)} \delta(\theta_\gamma, \eta_\gamma), \quad (17)$$

$$\frac{\partial u_{\gamma,\alpha}(\theta_\gamma)}{\partial b_\alpha(\eta_n, \eta_\gamma)} = -\frac{u_\alpha(\eta_n, \theta_\gamma) \sin \eta_\gamma}{d_\alpha(\eta_n, \theta_\gamma) - b_\alpha(\eta_n, \theta_\gamma)} \delta(\theta_\gamma, \eta_\gamma), \quad (18)$$

$$\frac{\partial u_{\gamma,\alpha}(\theta_\gamma)}{\partial \rho_{n,\alpha}(\eta_n)} = -\frac{u_\alpha(\eta_n, \theta_\gamma) \sin \eta_\gamma}{\rho_{n,\alpha}(\eta_n)} \delta(\theta_\gamma, \eta_\gamma), \quad (19)$$

$$\frac{\partial u_{\gamma,\alpha}(\theta_\gamma)}{\partial \psi_{n,\alpha}(\eta_n)} = \frac{u_\alpha(\eta_n, \theta_\gamma) \sin \eta_\gamma}{\psi_{n,\alpha}(\eta_n)} \delta(\theta_\gamma, \eta_\gamma). \quad (20)$$

There are two important differences here between the n and γ distributions: First, the lack of a dependence on γ -detection angle for $\rho_{n,\alpha}(\theta_n)$ and $\psi_{n,\alpha}(\theta_n)$ generates a correlation between different γ -detection angles for the unnormalized distributions. Second, whereas in Eqs. (8) and (9) the derivatives with respect to $\rho_{n,\alpha}(\theta_n)$ and $\psi_{n,\alpha}(\theta_n)$ pull out factors of $u_{n,\alpha}(\theta_n)$, here derivatives with respect to these parameters pull out the much smaller factors of $u_\alpha(\theta_n, \theta_\gamma)$, both of which are squared in the covariances. This second difference leads to a much smaller dependence of the covariance of the γ distributions on the variance of $\rho_{n,\alpha}(\theta_n)$ and $\psi_{n,\alpha}(\theta_n)$ than for the n distributions. The area of each γ distribution is calculated identically as in Eq. (12), and thus the normalized distribution has an identical form to that of Eq. (12). An example normalized correlation matrix corresponding to the γ distribution for $E_\alpha = 13.80\text{--}14.13$ MeV is shown in Fig. 8.

3. Correlated $n\text{-}\gamma$ Distributions

The unnormalized correlated $n\text{-}\gamma$ distribution calculated from Eq. (3) has a covariance described by

$$\begin{aligned} \text{cov} [u_\alpha(\theta_n, \theta_\gamma), u_\alpha(\phi_n, \phi_\gamma)] &= \left(\frac{\partial u_\alpha(\theta_n, \theta_\gamma)}{\partial d_\alpha(\eta_n, \eta_\gamma)} \right)^2 \text{var} [d_\alpha(\theta_n, \eta_\gamma)] \delta(\theta_n, \phi_n) \delta(\theta_\gamma, \phi_\gamma) \\ &\quad + \left(\frac{\partial u_\alpha(\theta_n, \theta_\gamma)}{\partial b_\alpha(\eta_n, \eta_\gamma)} \right)^2 \text{var} [b_\alpha(\theta_n, \eta_\gamma)] \delta(\theta_n, \phi_n) \delta(\theta_\gamma, \phi_\gamma) \\ &\quad + \left(\frac{\partial u_\alpha(\theta_n, \theta_\gamma)}{\partial \rho_{n,\alpha}(\eta_n)} \right) \left(\frac{\partial u_\alpha(\theta_n, \phi_\gamma)}{\partial \rho_{n,\alpha}(\eta_n)} \right) \\ &\quad \times \text{var} [\rho_{n,\alpha}(\eta_n)] \delta(\theta_n, \phi_n) \\ &\quad + \left(\frac{\partial u_\alpha(\theta_n, \theta_\gamma)}{\partial \psi_{n,\alpha}(\eta_n)} \right) \left(\frac{\partial u_\alpha(\theta_n, \phi_\gamma)}{\partial \psi_{n,\alpha}(\eta_n)} \right) \\ &\quad \times \text{var} [\psi_{n,\alpha}(\eta_n)] \delta(\theta_n, \phi_n), \end{aligned} \tag{21}$$

with derivatives calculated similarly as in the previous sections. This covariance matrix is also generally non-diagonal.

To normalize the correlated $n\text{-}\gamma$ distribution shown Eq. (3), the volume of the two-dimensional distribution shape must be calculated instead of the area as in Secs. III E 1 and III E 2. The volume of this distribution can be calculated by considering each six- or seven-sided polygon created by the eight points with $[x, y, z] = [\theta_n, \theta_\gamma, 0]$, $[\theta_n + \Delta_\theta, \theta_\gamma, 0]$, $[\theta_n, \theta_\gamma + \Delta_\theta, 0]$, $[\theta_n + \Delta_\theta, \theta_\gamma + \Delta_\theta, 0]$, $[\theta_n, \theta_\gamma, u_\alpha(\theta_n, \theta_\gamma)]$, $[\theta_n + \Delta_\theta, \theta_\gamma, u_\alpha(\theta_n + \Delta_\theta, \theta_\gamma)]$, $[\theta_n, \theta_\gamma + \Delta_\theta, u_\alpha(\theta_n, \theta_\gamma + \Delta_\theta)]$, and $[\theta_n + \Delta_\theta, \theta_\gamma + \Delta_\theta, u_\alpha(\theta_n + \Delta_\theta, \theta_\gamma + \Delta_\theta)]$. Again, Δ_θ is the difference in polar angle between each detector in the lab frame, which is 15° for the detector array used here. The first four points of this shape represent the square “base” of the shape in the $u_\alpha(\theta_n, \theta_\gamma) = 0$ plane, and the remaining four points are the corners formed by each angular distribution point. For one of these shapes, the volume can be calculated generally by

$$\begin{aligned} v_\alpha = \frac{\Delta_\theta^2}{8} \Big\{ &2u_\alpha(\theta_n, \theta_\gamma) + 2u_\alpha(\theta_n + \Delta_\theta, \theta_\gamma + \Delta_\theta) \\ &+ u_\alpha(\theta_n + \Delta_\theta, \theta_\gamma) + u_\alpha(\theta_n, \theta_\gamma + \Delta_\theta) \\ &+ \min [u_\alpha(\theta_n, \theta_\gamma), \\ &\quad u_\alpha(\theta_n + \Delta_\theta, \theta_\gamma), \\ &\quad u_\alpha(\theta_n + \Delta_\theta, \theta_\gamma + \Delta_\theta)] \\ &+ \min [u_\alpha(\theta_n, \theta_\gamma), \\ &\quad u_\alpha(\theta_n, \theta_\gamma + \Delta_\theta), \\ &\quad u_\alpha(\theta_n + \Delta_\theta, \theta_\gamma + \Delta_\theta)] \Big\}. \end{aligned} \tag{22}$$

From this expression it is clear that the number of instances of any given $u_\alpha(\theta_n, \theta_\gamma)$ depends on the relative values of the distribution, and will therefore not generally be constant for a given E_α . To simplify the presentation of the total volume of this correlated $n\text{-}\gamma$ distribution, we introduce a variable $N_\alpha(\theta_n, \theta_\gamma)$ for each $u_\alpha(\theta_n, \theta_\gamma)$ denoting the total number of instances of $u_\alpha(\theta_n, \theta_\gamma)$ across the total volume of the distribution for E_α . Thus, the total volume of the distribution can be written as

$$V_\alpha = \frac{\Delta_\theta^2}{8} \sum_{i=1}^{\Theta} \sum_{j=1}^{\Theta} N_\alpha(\theta_{n,i}, \theta_{\gamma,j}) u_\alpha(\theta_{n,i}, \theta_{\gamma,j}). \tag{23}$$

The normalized correlated $n\text{-}\gamma$ distribution can now be calculated as

$$n_\alpha(\theta_n, \theta_\gamma) = \frac{u_\alpha(\theta_n, \theta_\gamma)}{V_\alpha}. \tag{24}$$

This expression leads to the normalized covariance expression

$$\begin{aligned} & \text{cov} [n_\alpha(\theta_n, \theta_\gamma), n_\alpha(\phi_n, \phi_\gamma)] \\ &= \sum_{i,j,k,l=1}^{\Theta} \left(\frac{\partial n_\alpha(\theta_n, \theta_\gamma)}{\partial u_\alpha(\eta_n, i, \eta_\gamma, j)} \right) \left(\frac{\partial n_\alpha(\phi_n, \phi_\gamma)}{\partial u_\alpha(\omega_n, k, \omega_\gamma, l)} \right) \\ & \quad \times \text{cov} [u_\alpha(\eta_n, i, \eta_\gamma, j), u_\alpha(\omega_n, k, \omega_\gamma, l)], \end{aligned} \quad (25)$$

with derivatives defined by

$$\begin{aligned} \frac{\partial n_\alpha(\theta_n, \theta_\gamma)}{\partial u_\alpha(\eta_n, \eta_\gamma)} &= \frac{\delta(\theta_n, \eta_n) \delta(\theta_\gamma, \eta_\gamma)}{V_\alpha} \\ & - \frac{u_\alpha(\eta_n, \eta_\gamma)}{V_\alpha^2} \frac{\Delta_\theta^2}{8} N_\alpha(\eta_n, \eta_\gamma) \end{aligned} \quad (26)$$

An example normalized correlation matrix of the correlated n - γ distribution corresponding to $E_\alpha = 13.80\text{--}14.13$ MeV is shown in Fig. 9. The high correlation between the distribution points within any n -detection angle implies that the shape of the γ distribution for each n -detection angle is more precisely defined than the one-dimensional uncertainties of each data point might indicate [36].

IV. RESULTS

In this section we present results for the normalized n distributions in Sec. IV A, γ distributions in Sec. IV B, and correlated n - γ distributions in Sec. IV C.

A. n Distributions

The present results for normalized n distributions are shown in Figs. 10(a) – 10(f) for the incident neutron energies $E_\alpha = 6.61\text{--}6.76$, $7.59\text{--}7.76$, $8.91\text{--}9.12$, $10.47\text{--}10.72$, $13.80\text{--}14.13$, and $15.49\text{--}15.85$ MeV alongside ENDF/B-VIII.0 [2] evaluations at relevant energies and available literature data sets. In every case, the present results were scaled to have the same area over the measured angular range as the average of the ENDF/B-VIII.0 distribution shown as the solid, black and dotted, red lines (i.e., those closest to the centroid of the measured E_α range). The distributions have been converted to the center-of-mass neutron angle, $\tilde{\theta}_n$.

In general, the data agree well with both the evaluations and the previously measured data. At $E_\alpha = 6.61\text{--}6.76$ MeV the data of Galati *et al.* [37] are towards the lower edge of the plotted incident neutron energy range, and so a disagreement in magnitude is expected. It is worth noting that the data of Galati *et al.* are the only n data considered for the ENDF/B-VIII.0 evaluation of the $^{12}\text{C}(n,n'\gamma)$ cross section; all other data sets considered contain γ data only. Conversely, Velkley *et al.* [38], shown in Fig. 10(b), don't seem to agree in shape or magnitude with nearby evaluations. The present measurements on the same plot appear to reasonably represent a convolution of the plotted ENDF/B-VIII.0 evaluation trends. However, the higher-statistics data from Velkley *et al.* [38] in Fig. 10(c) agree well with those of Glasgow *et al.* [39], Haouat *et al.* [40], ENDF/B-VIII.0, and the present results. Similar agreement was found with Glasgow *et al.* and Haouat *et al.* in Fig. 10(d). There are a large number measurements of the $Q = 4.4398$ MeV $^{12}\text{C}(n,n'\gamma)$ reaction at $E_\alpha \approx 14$ MeV, and we show only a portion of the available data in Fig. 10(e) [41–50]. While there are some disagreements between data sets, the n distribution at this incident neutron energy appears well established, and the present results agree well with that trend. Finally, in Fig. 10(f) we compare to one of the only available data sets above $E_\alpha = 14$ MeV, those of Chen *et al.* [51], and we once again see good agreement between literature data, the ENDF/B-VIII.0 evaluation, and the present results across the measured angular range.

B. γ Distributions

There are far fewer data sets available for γ distributions from the $Q = 4.4398$ MeV $^{12}\text{C}(n,n'\gamma)$ reaction than for neutrons. Specifically, the data from Wender *et al.* [52] were reported from $E_\alpha = 5\text{--}25$ MeV in the form of Legendre

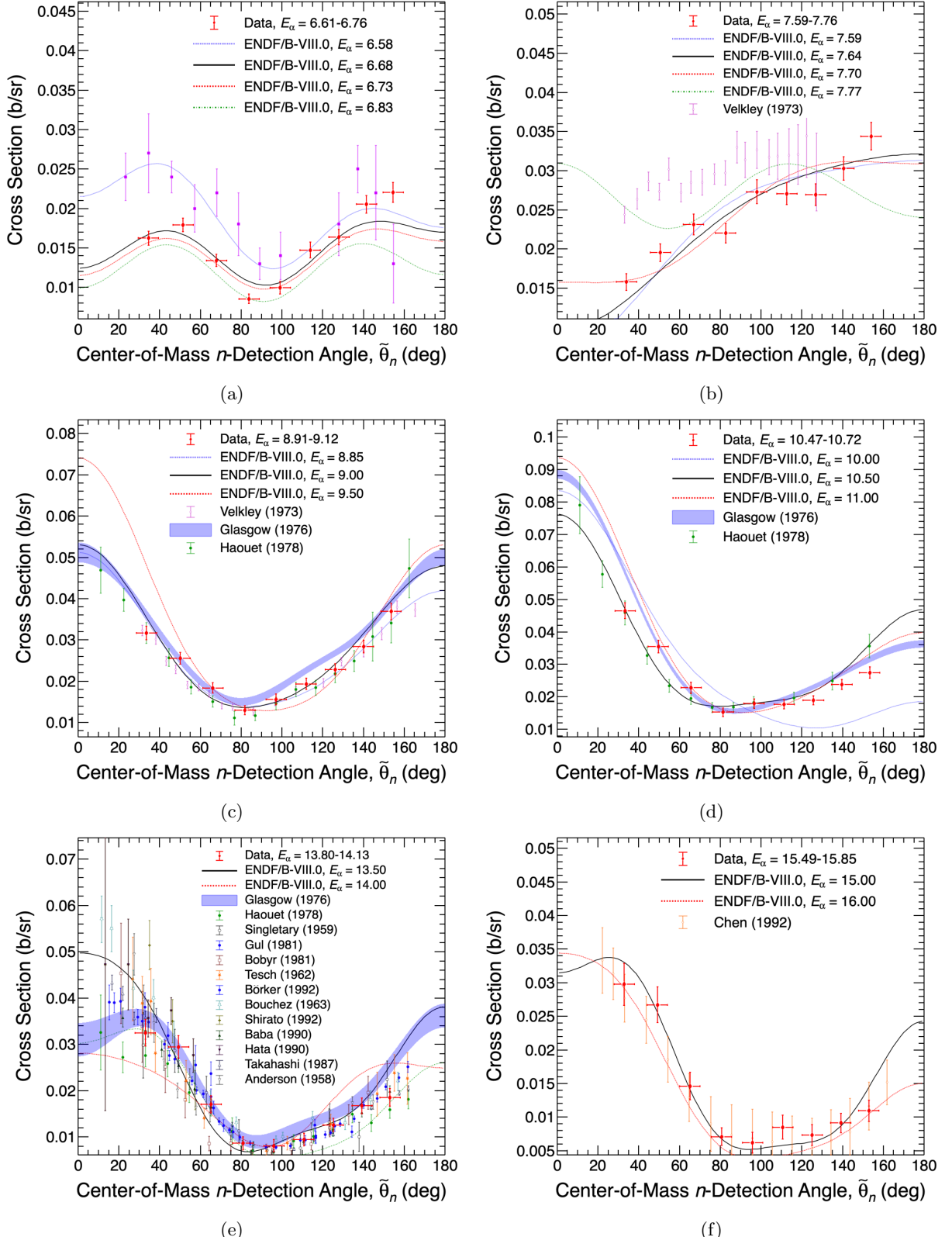


FIG. 10: Results for normalized n distributions are shown for $E_\alpha = 6.61\text{--}6.76$ MeV in panel (a), $7.59\text{--}7.76$ MeV in panel (b), $8.91\text{--}9.12$ MeV in panel (c), $10.47\text{--}10.72$ MeV in panel (d), $13.80\text{--}14.13$ MeV in panel (e), and $15.49\text{--}15.85$ MeV in panel (f). All E_α values are in MeV. The present results are scaled to ENDF/B-VIII.0 evaluation as described in the text. Literature data E_α values in panel (e) are all near 14 MeV.

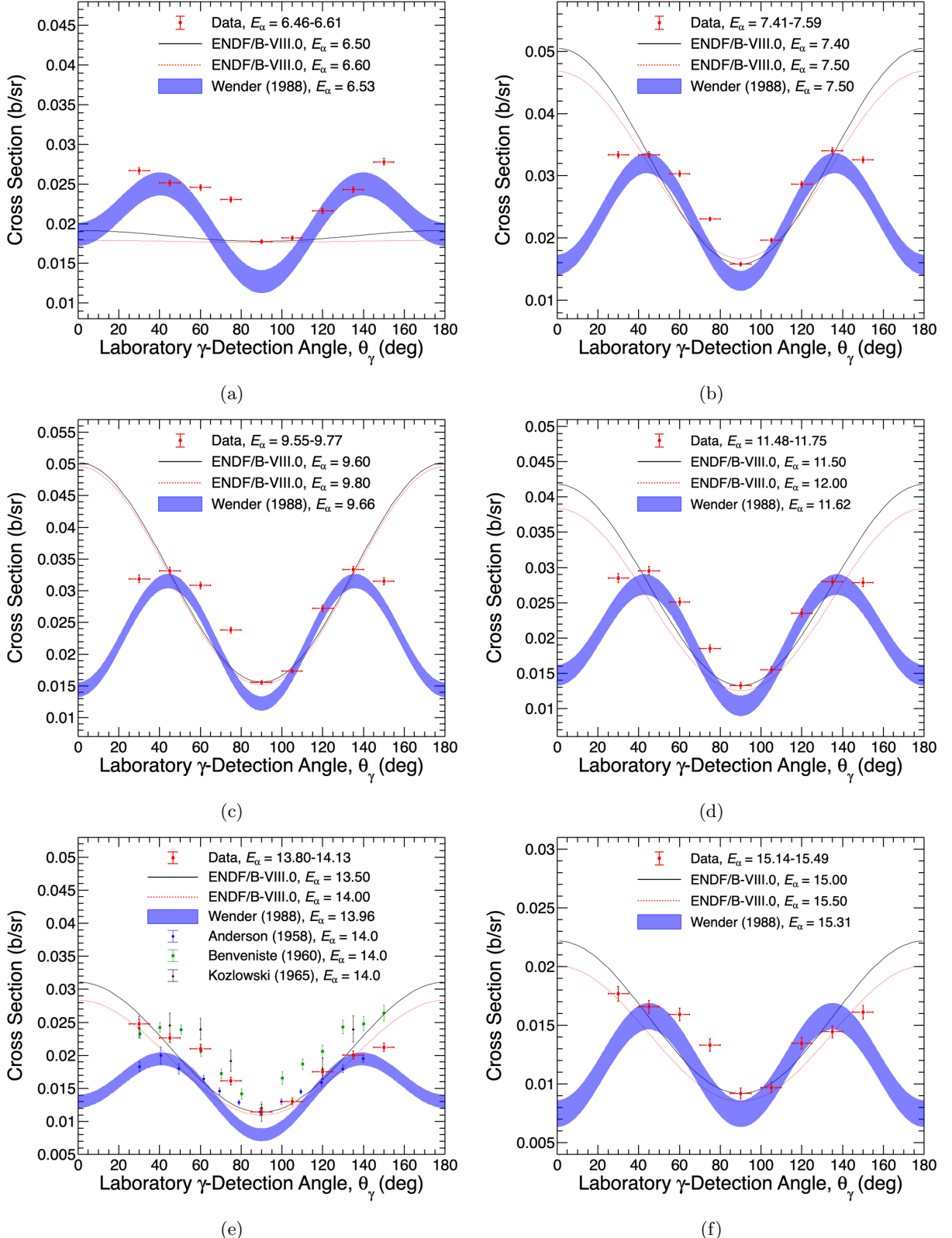


FIG. 11: Results for normalized γ distributions are shown for $E_\alpha = 6.46\text{--}6.61$ MeV in panel (a), $7.41\text{--}7.59$ MeV in panel (b), $9.55\text{--}9.77$ MeV in panel (c), $11.48\text{--}11.75$ MeV in panel (d), $13.80\text{--}14.13$ MeV in panel (e), and $15.14\text{--}15.49$ MeV in panel (f). All E_α values are in MeV. The present results are scaled to ENDF/B-VIII.0 evaluation as described in the text.

polynomial coefficients. These data are shown in Figs. 11(a) – 11(f) along with the present results and nearby ENDF/B-VIII.0 evaluations. At $E_\alpha \approx 14$ MeV, we also compare with the data of Anderson *et al.* [41], Benveniste *et al.* [42], and Kozlowski *et al.* [53].

The data of Wender *et al.* definitively suggest a significant a_4 Legendre polynomial coefficient, which creates the decrease in the angular distribution towards extreme forward and backward angles. The ENDF/B-VIII.0 evaluation does not appear to incorporate this component, and as a result the angular distribution from Wender *et al.* strongly disagrees with ENDF/B-VIII.0 at these extreme angles. This is interesting considering the use of the data from Wender *et al.* as shape data in the ENDF/B-VIII.0 evaluated $^{12}\text{C}(n,n'\gamma)$ cross section. It is similarly surprising, that Wender *et al.* reported such strong a_4 coefficients when they measured the distribution at five angles over a range of $\theta_\gamma = 40\text{--}140^\circ$. Nevertheless, the present results do indicate the presence of a notable a_4 Legendre polynomial component for the γ distribution from this reaction through the presence of a similar downturn at extreme angles as that observed by Wender *et al.*. The existence of this feature is clear even without Legendre polynomial fits to the data. In fact, all other literature data sets shown at $E_\alpha \approx 14$ MeV also show some signature of this same decrease in the angular distribution at towards extreme angles. Considering these facts, it seems likely that a nonzero a_4 component for the γ distributions from this reaction is more realistic than the distributions currently existing in ENDF/B-VIII.0.

C. Correlated n - γ Distributions

Finally, we address the correlated n - γ distributions. There are only three publications of the correlated n - γ distributions from the $Q = 4.4398$ MeV $^{12}\text{C}(n,n'\gamma)$ reaction known to the authors: Benetski *et al.* [9], Zamudio *et al.* [10], and Spaargaren *et al.* [11]. To match the presentation of the literature data, we compare the present γ distributions correlated to different θ_n values with the available literature data at the same or similar θ_n values in Figs. 12(a) – 12(f). There does not appear to be general agreement of the present results with the literature data at any θ_n value. At $\theta_n = 30^\circ$ Zamudio *et al.* may suggest a minimum in the distribution near $\theta_\gamma \approx 90^\circ$ as is seen in the present results in Fig. 12(a), and the same may be true for the literature data shown at $\theta_n = 45^\circ$ in Fig. 12(b). However, in Figs. 12(c) – 12(f) the literature data appear to show maxima and minima of the γ distributions that are not seen in the present results.

At each of the forty E_α ranges measured for this work, we have obtained a clear measure of the correlated n - γ distribution from this reaction. For a single E_α it is convenient to consider these data as a two-dimensional histogram of θ_n vs θ_γ , as is shown in Fig. 13 for $E_\alpha = 9.77\text{--}10.00$ MeV. However, it is not practical to show such a plot for each measured E_α range, and in some cases it is difficult to see how the distributions at each θ_n and θ_γ change with this plotting style. Thus, we instead display the data as n distributions at each θ_γ and each E_α in Fig. 14, and also as γ distributions for each θ_n and each E_α in Fig. 15. Note that the uncertainties are not shown on these plots to make it easier to see the centroids of the various distributions, though the uncertainties in Figs. 12(a) – 12(f) give an estimate of the uncertainties obtained for these distributions.

Perhaps the most interesting features in the correlated n - γ distributions occur from $E_\alpha = 7.0\text{--}8.0$ MeV. Over this energy range the thresholds for both the $Q = 7.6541$ $^{12}\text{C}(n,n'\gamma)$ reaction and the $^{12}\text{C}(n,n')3\alpha$ breakup reaction are crossed. The emergence of these new reaction channels creates significant differences in the n distributions between the forward and backward angles depending on the γ -detection angle. At $E_\alpha = 7.41\text{--}7.59$ MeV and $\theta_\gamma = 90^\circ$ there is nearly a factor of 3 increase in the n distribution going from 30° to 150° , whereas the n distribution is effectively flat across all measured angles at $\theta_\gamma = 30^\circ$ and 150° . These features can also be seen in the same E_α ranges for the γ distributions; the clear dipole transition shape at forward θ_n values complements the dip in the n distribution at $\theta_n = 30^\circ$ and $\theta_\gamma = 90^\circ$, and the nearly flat or perhaps even 90° -peaked γ distribution at backward θ_n values shows the flat n distribution for these γ -detection angles.

At higher E_α values the n distributions tend to be peaked towards forward angles, with the caveat that the distributions become flatter when correlated with a θ_γ near 90° . The γ distributions show an analogous pattern, displaying clear dipole transition angular distributions when correlated with both forward and the most extreme backward θ_n angles, and instead becoming flatter towards $\theta_n \approx 90^\circ$. As a final comment on these distributions, we note that there are no nuclear data evaluation comparisons on Figs. 14 and 15 because no such evaluations exist. However, knowledge of these correlations would be essential for any measurement involving, for example, tagging on inelastic neutrons using only a single or a small number of θ_γ values.

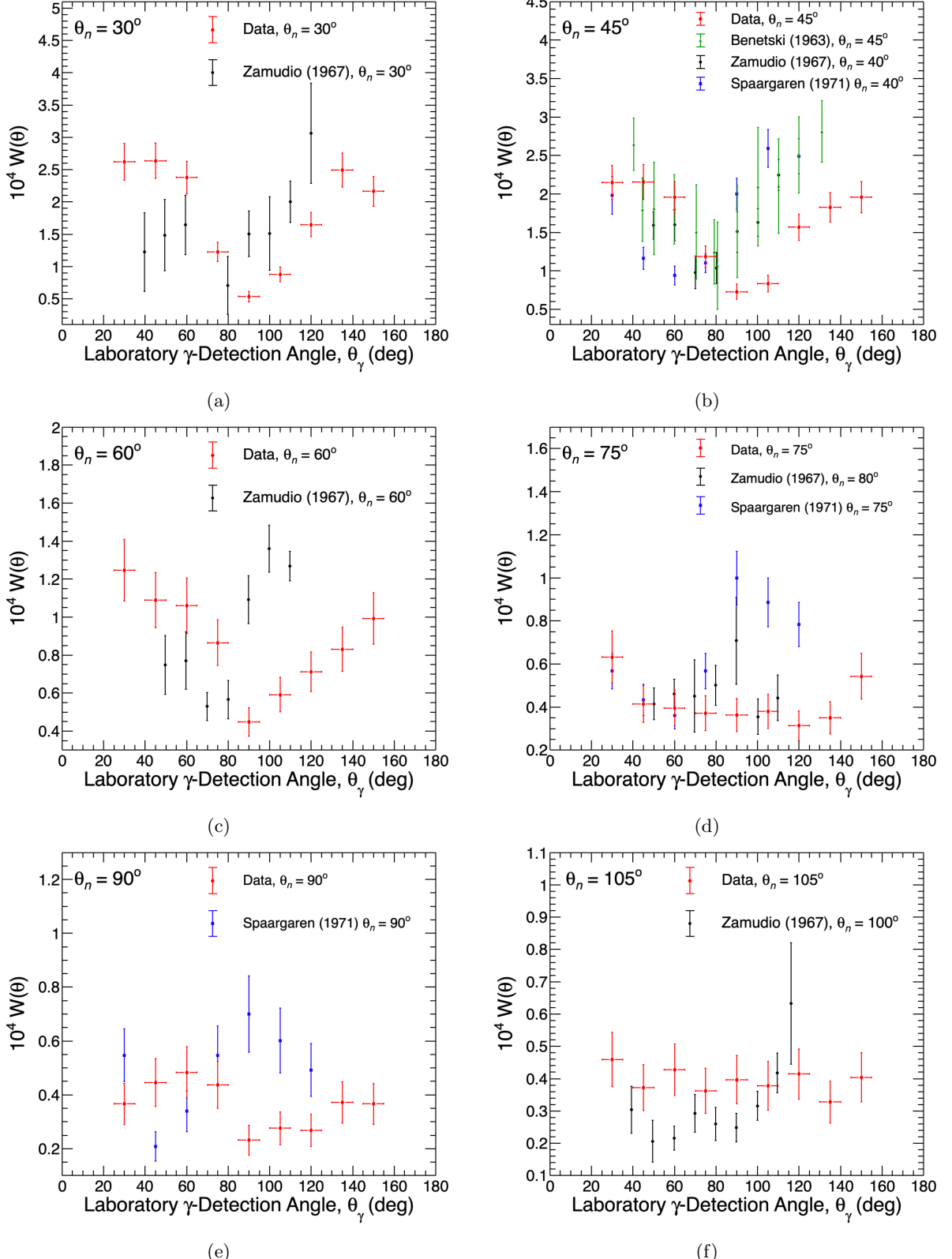


FIG. 12: The results for the normalized correlated n- γ distribution data at $E_\alpha \approx 14$ MeV are shown here as γ distributions compared to the available literature data for $\theta_n = 30^\circ$ in panel (a), $\theta_n = 45^\circ$ in panel (b), $\theta_n = 60^\circ$ in panel (c), $\theta_n = 75^\circ$ in panel (d), $\theta_n = 90^\circ$ in panel (e), and $\theta_n = 105^\circ$ in panel (f). The literature data on these plots are scaled to the present results.

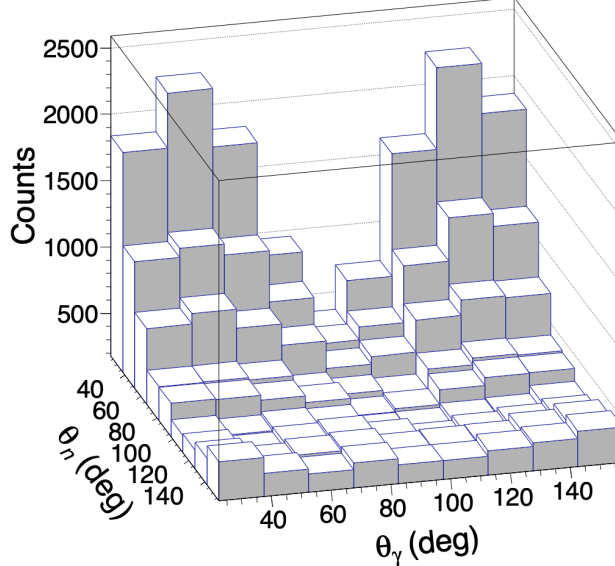


FIG. 13: (color online) A three-dimensional representation of a correlated n - γ distribution corresponding to $E_\alpha = 9.77\text{--}10.00$ MeV.

V. CONCLUSIONS

The n , γ , and correlated n - γ distributions from the $Q = 4.4398$ MeV $^{12}\text{C}(n,n'\gamma)$ reaction have been measured for continuous incident energies ranging from 6.5–16.5 MeV. All previous measurements of the correlated n - γ distributions were at or near 14 MeV incident energy, and so this work is the first of its kind. We also describe a detailed covariance description of these angular distributions including their treatment as normalized probability distributions. The n distributions, effectively integrated over γ -detection angle in that the γ emission was not observed, have been measured by many authors, especially near 14 MeV incident neutron energy. Our results largely agree with both the experimental data and nuclear data evaluations. The γ distributions, analogously integrated over n -detection angle, show a decreasing trend going towards extreme γ -detection angles, which indicates a non-negligible a_4 contribution to a Legendre polynomial description of these distributions. This decrease is not included in the ENDF/B-VIII.0 nuclear data evaluation, but it is supported by the limited number of available data sets on the γ distributions from this reaction.

The only available comparisons for correlated n - γ distributions are three experimental measurements at 14 MeV incident neutron energy and at specific combinations of n - and γ -detection angle. No nuclear data evaluations of these correlated distributions exist. In general, our results do not agree with the available experimental data, though these literature data contain large statistical fluctuations and may contain lingering systematic errors. In this work we show the n distribution observed when correlated with each γ -detection angle for each of the forty incident neutron energy ranges from 6.5–16.5 MeV, as well as the γ distribution observed when correlated with each n -detection angle for the same incident energy ranges. In some cases, these distributions have dramatically different shapes depending on the angle of the correlated particle, especially near thresholds for the opening of other reaction channels, such as the $Q = 7.6541$ $^{12}\text{C}(n,n'\gamma)$ reaction and the $^{12}\text{C}(n,n')3\alpha$ breakup reaction in this case. These changes in the correlated angular distributions can have important implications for experiments that tag on inelastic scattering reactions using a single or small number of γ -detection angles, potentially yielding large systematic errors in the data if a single distribution is assumed.

VI. ACKNOWLEDGEMENTS

The authors would like to thank Toshihiko Kawano and Mark Paris for informative discussions on modern scattering theories and data evaluation efforts, as well as Yaron Danon and Kumar Mohindroo for allowing our use of their target-changing system. Funding for the authors of this work was provided by the Laboratory Directed Research and

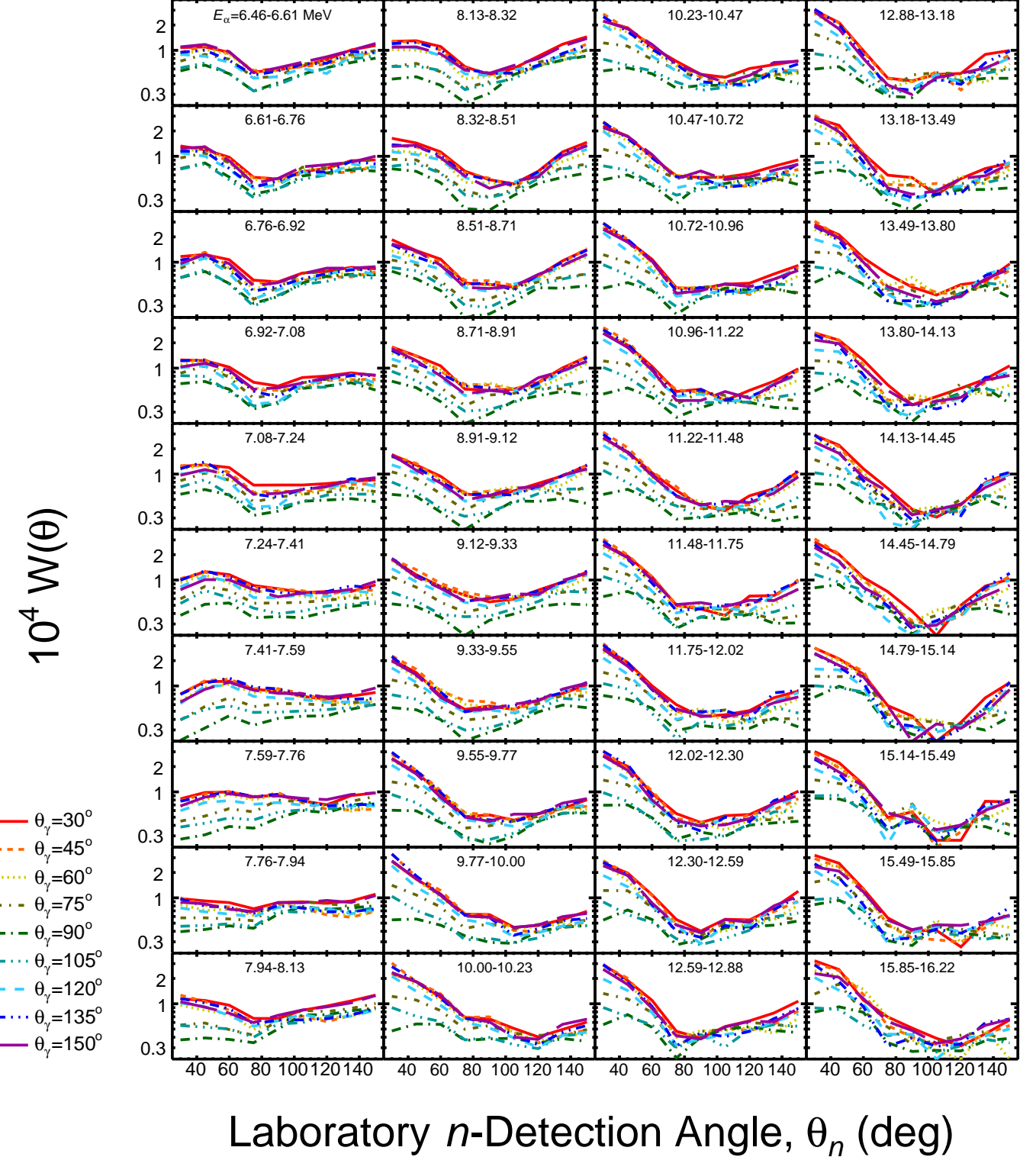


FIG. 14: (color online) Two-dimensional representations of the measured normalized correlated n - γ distributions with separate n distributions for each θ_γ . Laboratory angles are shown along the x axis for consistency between the plots of n and γ distributions. Note that uncertainties are not shown on the data in these figures.

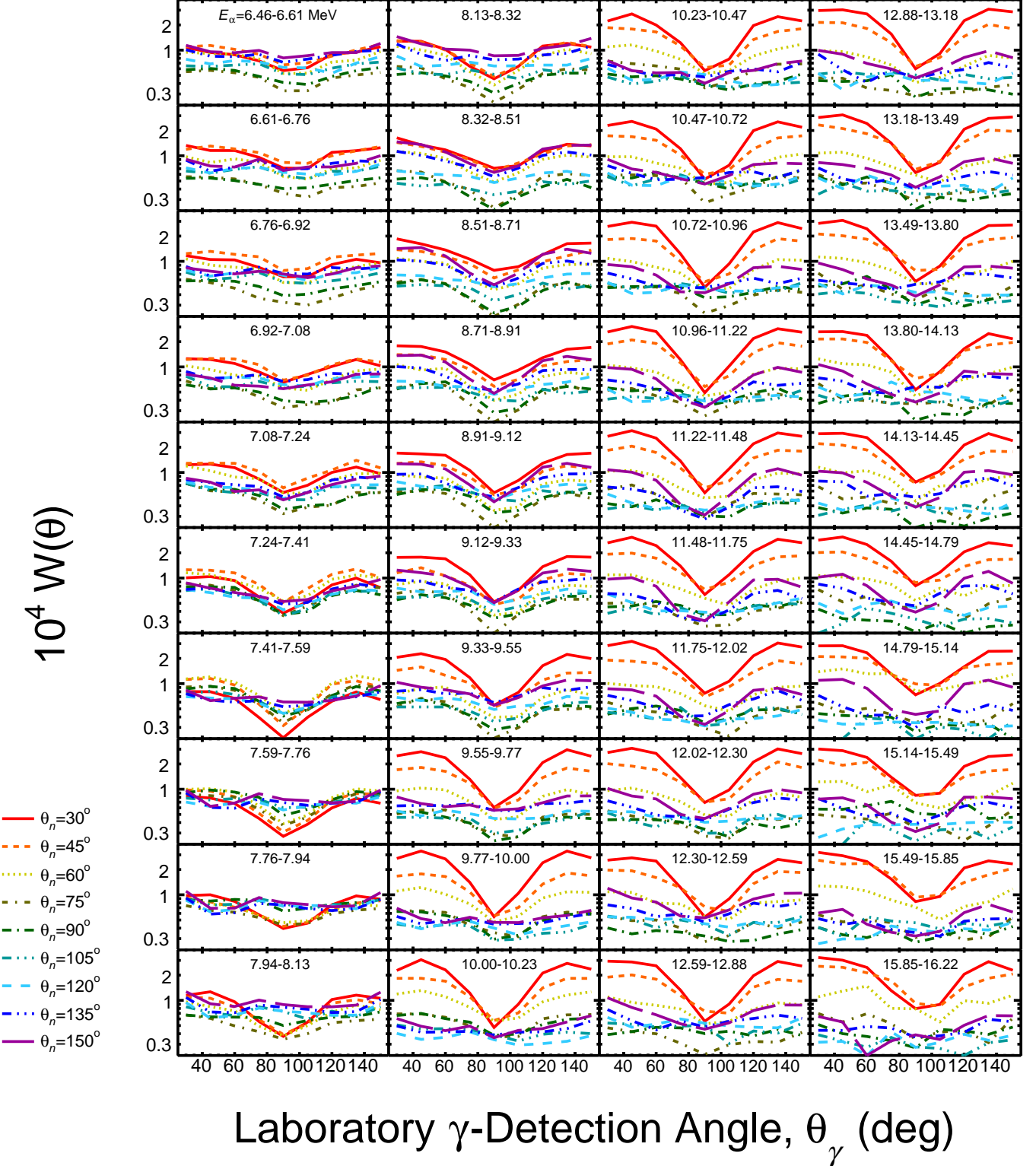


FIG. 15: (color online) Two-dimensional representations of the measured normalized correlated n - γ distributions with separate γ distributions for each θ_n . Laboratory angles are shown along the x axis for consistency between the plots of n and γ distributions. Note that uncertainties are not shown on the data in these figures.

Development program at Los Alamos National Laboratory under award number 20210329ER. Additional funding for K. J. Kelly was provided by award number 20190588ECR. This work was also funded by the U.S. Department of Energy through Los Alamos National Laboratory. Los Alamos National Laboratory is operated by Triad National Security, LLC, for the National Nuclear Security Administration of the U.S. Department of Energy (Contract No. 89233218CNA000001).

- [1] M. B. Chadwick, E. Dupont, E. Bauge, A. Blokhin, O. Bouland, *et al.*, Nucl. Data Sheets **118**, 1 (2014).
- [2] D. A. Brown, M. B. Chadwick, R. Capote, A. C. Kahler, A. Trkov, *et al.*, Nucl. Data Sheets **148**, 1 (2018).
- [3] R. C. Haight, J. M. O'Donnell, L. Zanini, M. Devlin, and D. Rochman, Proceedings of the 11th International Symposium on Capture Gamma-Ray Spectroscopy and Related Topics, LA-UR-02-5486.
- [4] D. Rochman, R. C. Haight, J. M. O'Donnell, M. Devlin, T. Ethvignot, and T. Granier, Nucl. Instrum. Methods A **523**, 102 (2004).
- [5] D. Rochman, R. C. Haight, J. M. O'Donnell, M. Devlin, T. Ethvignot, *et al.*, AIP Conf. Proc. **769**, 985 (2005).
- [6] G. Hale and M. Paris, Nucl. Data Sheets **123**, 165 (2015), Special Issue on International Workshop on Nuclear Data Covariances April 28 - May 1, 2014, Santa Fe, New Mexico, USA <http://t2.lanl.gov/cw2014>.
- [7] C. R. Brune and R. J. deBoer, Phys. Rev. C **102**, 024628 (2020).
- [8] C. J. Werner, J. Armstrong, F. B. Brown, J. S. Bull, L. Casswell, *et al.*, LA-UR-17-29981 (2017).
- [9] B. A. Benetski and I. M. Frank, Sov. Phys. JETP **44**, 454 (1963).
- [10] J. Zamudio, L. Romero, and R. Morales, Nucl. Phys. A **96**, 449 (1967).
- [11] D. Spaargaren and C. C. Jonker, Nucl. Phys. A **161**, 354 (1971).
- [12] J. H. Kelley, J. E. Purcell, and C. G. Sheu, Nucl. Phys. A **71**, 968 (2017).
- [13] J. Zhang, Y. Han, and L. Cao, Nucl. Sci. Eng. **133**, 218 (1999).
- [14] R. Smith, T. Kokalova, C. Wheldon, J. E. Bishop, M. Freer, *et al.*, Phys. Rev. Lett. **119**, 132502 (2017).
- [15] M. Devlin, J. A. Gomez, K. J. Kelly, R. C. Haight, J. M. O'Donnell, *et al.*, Nucl. Data Sheets **148**, 322 (2018).
- [16] K. J. Kelly, J. A. Gomez, J. M. O'Donnell, M. Devlin, R. C. Haight, *et al.*, Proceedings of the 20th Topical Meeting of the Radiation Protection and Shielding Division, LA-UR-18-28140 (2018).
- [17] K. J. Kelly, M. Devlin, J. M. O'Donnell, J. A. Gomez, D. Neudecker, *et al.*, Phys. Rev. C **102**, 034615 (2020).
- [18] K. J. Kelly, P. Marini, J. Taieb, M. Devlin, D. Neudecker, *et al.*, Nucl. Data Sheets **173**, 42 (2021).
- [19] <https://eljentechnology.com/products/liquid-scintillators/ej-301-ej-309>.
- [20] <https://www.hamamatsu.com>.
- [21] <https://www.caen.it/products/sy4527> (2020).
- [22] <https://www.caen.it/products/v1730> (2020).
- [23] <http://npg.dl.ac.uk/MIDAS>.
- [24] J. M. O'Donnell, Nucl. Instrum. Methods A **805**, 87 (2016).
- [25] C. J. Solomon, C. Bates, and J. Kulesza, LA-UR-17-21779 (March 30, 2017).
- [26] T. N. Taddeucci, R. C. Haight, H. Y. Lee, D. Neudecker, J. M. O'Donnell, *et al.*, Nucl. Data Sheets **123**, 135 (2015).
- [27] K. J. Kelly, J. M. O'Donnell, J. A. Gomez, T. N. Taddeucci, M. Devlin, *et al.*, Nucl. Instrum. and Methods A **866**, 182 (2017).
- [28] K. J. Kelly, M. Devlin, J. A. Gomez, J. M. O'Donnell, T. N. Taddeucci, *et al.*, EPJ Web of Conferences **193**, 03003 (2018).
- [29] K. J. Kelly, J. A. Gomez, J. M. O'Donnell, M. Devlin, R. C. Haight, *et al.*, Nucl. Instrum. and Methods A **954**, 161411 (2020).
- [30] A. Lajtai, P. P. Dyachenko, V. N. Kononov, and E. A. Seregina, Nucl. Instrum. and Methods A **293**, 555 (1990).
- [31] C. C. Lawrence, A. Enqvist, M. Flaska, S. A. Pozzi, and F. D. Bechetti, Nucl. Instrum. and Methods A **729**, 924 (2013).
- [32] B. Pehlivanovic, S. Avdic, P. Marinkovic, S. A. Pozzi, and M. Flaska, Rad. Meas. **49**, 109 (2013).
- [33] M. Febrarro, R. Toomey, S. D. Pain, K. A. Chipp, B. Becker, *et al.*, Nucl. Instrum. Methods A **946**, 162668 (2019).
- [34] M. Febrarro, B. Becker, R. J. deBoer, K. Brandenburg, C. Brune, *et al.*, Nucl. Instrum. Methods A **989**, 164824 (2021).
- [35] D. Neudecker, R. Capote, D. L. Smith, and T. Burr, Nucl. Sci. Eng. **179**, 381 (2015).
- [36] K. J. Kelly, J. M. O'Donnell, D. Neudecker, M. Devlin, and J. A. Gomez, Nucl. Instrum. and Methods A **943**, 162449 (2019).
- [37] W. Galati, J. D. Brandenberger, and J. L. Weil, Phys. Rev. C **5**, 1508 (1972).
- [38] D. E. Velkey, J. D. Brandenberger, D. W. Glasgow, M. T. McEllistrem, J. C. Manthuruthil, and C. P. Poirier, Phys. Rev. C **7**, 1736 (1973).
- [39] D. W. Glasgow, F. O. Purser, H. Hogue, J. C. Clement, K. Stelzer, and otheres, Nucl. Sci. Eng. **61**, 521 (1976).
- [40] G. Haouat, J. Lackhar, J. Sigaud, Y. Patin, and Coçu, Nucl. Sci. Eng. **65**, 331 (1978).
- [41] J. D. Anderson, C. C. Gardner, J. W. McClure, M. P. Nakada, and W. C., Phys. Rev. **111**, 572 (1958).
- [42] J. Benveniste, A. C. Mitchell, C. D. Schrader, and J. H. Zenger, Nucl. Phys. **19**, 448 (1960).
- [43] J. B. Singletary and D. E. Wood, Phys. Rev. **114**, 1595 (1959).
- [44] V. V. Bobyr, L. Y. Grona, and V. I. Strizhak, Sov. Phys. JETP **14**, 18 (1962).
- [45] K. Tesch, Nucl. Phys. **37**, 412 (1962).
- [46] K. Gul, M. Anwar, M. Ahmad, S. M. Saleem, and N. A. Khan, Phys. Rev. C **24**, 2458 (1981).

- [47] R. Bouchez, J. Duclos, and P. Perrin, Nucl. Phys. **43**, 623 (1963).
[48] J. H. Dave and C. R. Gould, Phys. Rev. C **28**, 2212 (1983).
[49] A. Negret, C. Borcea, P. Dessagne, M. Kerveno, N. Nankov, *et al.*, Nucl. Data Sheets **119**, 179 (2014).
[50] V. C. Rogers, V. J. Orphan, C. G. Hoot, and V. V. Verbinski, Nucl. Sci. Eng. **58**, 298 (1975).
[51] Z. M. Chen, K. Baird, C. R. Howell, M. L. Roberts, W. Tornow, and R. L. Walter, J. Phys. G **19**, 877 (1992).
[52] S. A. Wender, S. J. Seestrom-Morris, and R. O. Nelson, J. Phys. G: Nucl. Phys. **14**, S417 (1988).
[53] T. Kozlowski, W. Kusch, and J. Wojtkowska, Rept: Inst. Badan Jadr. (Nucl.Res.), Swierk+Warsaw, Report No.661 (1965), Poland, EXFOR Entry R,INR-661,196509 (1965).
[54] <https://www-nds.iaea.org/exfor>.

Appendix: Angular Distribution Data

We report tables of normalized $n\gamma$, n , and γ distribution data with uncertainties in Tabs. I, II, and III, respectively. Covariance data will be made available via EXFOR [54] following publication due to the large extent of these data.

TABLE I: The normalized correlated $n\gamma$ angular distributions measured in this work as a function of incident neutron energy, E_α , and laboratory n - and γ -detection angle. The uncertainty on all the laboratory γ -detection angles is $\pm 5^\circ$. The overall scaling of the $n\gamma$ distribution values is arbitrary.

		θ_n (deg)	Laboratory γ -Detection Angle (deg)								
			30	45	60	75	90	105	120	135	150
6.46–6.61	30	14.10(85)	12.28(73)	11.54(70)	9.75(62)	7.46(50)	8.07(54)	11.70(71)	12.37(74)	14.37(83)	
	45	14.35(82)	14.87(88)	13.37(78)	11.71(70)	8.73(56)	9.24(58)	11.11(67)	13.14(77)	15.35(87)	
	60	12.36(78)	11.90(75)	11.73(77)	10.26(67)	6.90(49)	6.95(50)	9.43(63)	9.94(65)	12.61(79)	
	75	7.23(56)	7.51(57)	7.03(54)	6.19(51)	4.28(37)	4.29(38)	6.09(49)	6.61(52)	7.08(55)	
	90	7.64(63)	7.90(64)	7.49(62)	6.37(54)	5.38(49)	5.09(45)	6.35(54)	7.44(61)	8.11(66)	
	105	8.51(65)	8.35(63)	8.68(65)	9.01(68)	6.81(54)	6.68(56)	7.97(61)	8.96(67)	9.44(70)	
	120	10.19(71)	8.96(64)	9.83(69)	9.48(67)	8.14(60)	8.03(59)	6.93(56)	9.17(66)	10.95(76)	
	135	13.22(88)	11.07(76)	10.92(75)	11.66(80)	9.36(67)	10.24(72)	11.35(78)	12.63(88)	13.06(87)	
	150	14.94(103)	12.51(90)	12.19(88)	12.98(92)	10.56(79)	11.26(83)	12.24(88)	12.24(88)	15.76(112)	
6.61–6.76	30	12.72(87)	11.07(75)	11.06(75)	9.17(64)	6.85(52)	6.76(51)	10.52(72)	11.03(75)	11.95(80)	
	45	11.45(73)	12.52(81)	11.57(74)	10.45(68)	7.99(55)	7.79(54)	9.59(63)	10.98(71)	12.37(78)	
	60	9.34(67)	7.97(58)	8.80(65)	8.04(59)	5.43(43)	5.04(41)	6.73(51)	6.87(52)	8.48(61)	
	75	5.39(48)	5.32(48)	5.07(46)	4.35(42)	3.42(34)	3.09(31)	3.99(38)	4.12(39)	4.56(42)	
	90	5.16(51)	5.20(51)	4.85(48)	4.37(44)	3.89(42)	3.98(41)	4.39(44)	4.87(48)	5.23(51)	
	105	6.30(55)	5.95(52)	6.60(57)	7.11(60)	5.60(50)	5.09(48)	6.26(54)	6.28(54)	7.19(61)	
	120	6.88(53)	5.97(47)	6.78(52)	6.96(54)	6.09(48)	5.78(46)	5.66(48)	6.25(49)	7.62(58)	
	135	8.49(63)	6.27(50)	7.00(54)	8.34(62)	6.62(52)	6.75(53)	7.80(59)	8.34(65)	8.14(61)	
	150	8.69(67)	7.23(58)	7.03(57)	8.72(67)	6.40(53)	7.04(57)	7.05(57)	7.79(61)	9.61(75)	
6.76–6.92	30	8.46(66)	7.62(58)	7.53(57)	6.13(49)	4.74(41)	4.76(41)	6.63(52)	7.66(58)	6.96(54)	
	45	8.95(64)	9.53(69)	8.78(63)	8.20(59)	5.63(45)	5.93(47)	8.12(59)	8.60(62)	8.99(64)	
	60	7.76(61)	6.53(53)	6.16(53)	5.91(49)	4.05(37)	3.99(37)	5.38(46)	6.29(52)	6.97(56)	
	75	4.43(44)	4.04(40)	3.46(36)	2.62(31)	2.35(27)	2.18(25)	2.64(29)	3.28(34)	3.80(39)	
	90	4.23(43)	4.29(43)	4.19(43)	3.63(38)	2.82(33)	2.94(32)	3.41(36)	3.72(39)	4.14(42)	
	105	5.39(48)	4.39(41)	4.62(42)	5.33(47)	4.10(39)	3.96(39)	4.25(40)	4.60(42)	5.29(47)	
	120	5.66(46)	4.83(41)	5.26(43)	5.63(46)	4.93(41)	4.29(37)	5.16(45)	5.31(44)	6.16(49)	
	135	6.29(50)	4.84(41)	5.28(44)	6.16(49)	5.20(44)	5.10(43)	6.10(49)	5.86(50)	6.16(50)	
	150	6.06(53)	5.53(49)	5.13(47)	5.52(49)	5.12(47)	4.63(43)	5.12(47)	6.08(53)	6.41(58)	
	30	8.36(65)	8.18(61)	7.33(56)	5.81(47)	4.37(38)	5.43(45)	6.76(53)	8.18(61)	6.89(54)	
	45	8.19(59)	8.40(62)	8.30(59)	7.09(52)	4.63(39)	5.32(43)	7.09(53)	8.29(59)	7.63(56)	
	60	6.87(54)	6.21(50)	5.32(46)	5.19(43)	3.74(34)	3.51(33)	4.72(40)	5.99(48)	6.30(51)	
	75	4.53(44)	3.67(37)	3.87(39)	2.93(33)	2.18(25)	2.37(27)	2.49(28)	3.55(36)	3.76(38)	

Continued on next page

TABLE I – *Continued from previous page*

		Laboratory γ -Detection Angle (deg)									
		30	45	60	75	90	105	120	135	150	
E_α		θ _n (deg)									
6.92–7.08	90	4.08(40)	3.64(37)	3.75(38)	3.34(34)	2.63(30)	2.52(28)	2.65(29)	3.02(32)	3.89(39)	
	105	5.16(47)	3.88(37)	3.87(37)	4.48(42)	3.83(37)	3.91(39)	4.31(41)	4.51(42)	4.45(42)	
	120	5.38(44)	4.77(40)	5.06(42)	4.92(41)	4.09(36)	3.97(35)	4.85(42)	5.02(42)	5.16(43)	
	135	5.87(47)	4.87(41)	5.00(41)	5.42(44)	4.48(38)	4.71(40)	5.58(45)	5.46(46)	5.80(47)	
	150	5.46(47)	4.92(43)	4.03(37)	3.93(36)	3.66(35)	4.07(37)	4.43(40)	5.45(46)	5.51(49)	
7.08–7.24	30	8.62(66)	8.77(64)	7.96(59)	5.82(47)	4.02(36)	4.91(41)	6.98(54)	8.09(60)	6.74(52)	
	45	8.97(61)	8.99(64)	8.96(61)	7.19(51)	4.57(37)	5.96(45)	7.46(53)	9.73(65)	7.89(55)	
	60	8.34(59)	7.30(53)	6.15(49)	5.88(45)	3.94(34)	3.97(34)	5.72(44)	6.72(50)	6.78(50)	
	75	5.15(45)	4.21(38)	4.06(37)	3.26(33)	2.25(24)	2.69(27)	2.83(28)	4.02(37)	4.01(37)	
	90	5.17(48)	4.39(42)	4.38(42)	3.71(37)	2.53(29)	2.80(30)	2.92(31)	3.70(37)	4.10(40)	
	105	5.17(46)	4.27(39)	4.01(37)	4.03(38)	3.31(32)	3.29(34)	4.75(43)	4.62(42)	4.54(41)	
	120	5.37(44)	4.60(39)	4.63(39)	4.23(37)	3.42(32)	3.92(35)	4.67(41)	4.95(42)	4.97(42)	
	135	5.73(46)	5.27(43)	4.97(41)	4.74(40)	3.56(32)	4.02(35)	5.68(45)	6.14(50)	5.85(47)	
	150	5.95(49)	5.34(45)	4.14(37)	4.32(38)	3.28(31)	4.02(36)	5.00(43)	5.82(48)	6.32(53)	
7.24–7.41	30	9.07(70)	9.39(69)	8.42(63)	5.38(45)	3.43(33)	4.74(41)	7.47(58)	9.00(67)	6.92(54)	
	45	11.34(72)	11.17(74)	10.38(67)	7.55(53)	4.64(37)	6.76(49)	9.99(65)	11.58(73)	9.12(61)	
	60	10.44(66)	9.89(63)	8.31(57)	6.83(47)	4.81(37)	5.56(41)	8.72(57)	9.78(62)	9.06(59)	
	75	7.76(55)	7.41(52)	6.41(47)	4.77(40)	3.21(29)	4.18(35)	5.57(42)	7.40(52)	6.91(50)	
	90	7.11(54)	7.09(54)	6.97(53)	4.82(40)	3.31(32)	3.60(32)	5.57(45)	6.41(50)	5.69(46)	
	105	6.39(49)	6.71(51)	5.77(45)	4.89(40)	3.22(29)	3.86(35)	6.03(47)	6.26(48)	6.31(48)	
	120	6.58(48)	6.04(45)	5.32(41)	5.18(40)	3.78(32)	4.43(36)	5.76(45)	6.57(48)	6.40(47)	
	135	6.60(48)	6.84(49)	5.87(44)	5.53(42)	4.38(35)	4.62(37)	6.67(48)	7.70(56)	6.98(50)	
	150	7.90(56)	6.82(50)	6.06(45)	5.45(42)	4.73(38)	5.00(39)	6.34(47)	7.22(52)	8.67(62)	
7.41–7.59	30	8.37(69)	8.32(66)	6.93(57)	4.10(38)	2.35(26)	4.13(38)	6.41(53)	8.27(65)	6.69(55)	
	45	11.67(76)	11.98(80)	10.01(67)	5.91(45)	3.29(30)	5.47(43)	10.29(68)	11.22(73)	9.47(64)	
	60	11.83(75)	12.53(79)	10.88(73)	7.52(53)	4.60(37)	6.03(45)	10.57(69)	12.87(80)	11.51(74)	
	75	9.49(62)	9.66(63)	8.66(57)	5.90(45)	3.56(30)	5.05(38)	7.82(53)	10.07(65)	9.26(61)	
	90	9.01(60)	9.64(63)	9.09(60)	6.40(46)	4.27(36)	5.07(39)	7.51(52)	9.60(63)	8.50(57)	
	105	7.82(53)	8.47(57)	7.72(53)	6.42(46)	4.55(35)	5.25(41)	7.16(50)	8.06(54)	8.41(56)	
	120	7.26(49)	7.00(47)	6.87(47)	6.09(43)	4.59(35)	5.45(39)	6.64(48)	7.70(51)	7.62(50)	
	135	7.86(52)	6.60(46)	6.25(44)	6.55(45)	5.51(40)	5.75(41)	6.73(46)	7.24(51)	8.28(54)	
	150	8.70(58)	6.51(46)	6.96(49)	7.23(50)	6.29(45)	6.24(45)	6.56(47)	7.38(51)	9.84(67)	
7.59–7.76	30	8.71(72)	8.25(67)	7.10(59)	4.72(43)	2.88(31)	4.02(39)	6.29(54)	8.16(66)	7.16(60)	
	45	10.34(73)	9.98(73)	8.54(62)	5.43(44)	3.25(31)	4.46(38)	7.85(58)	9.35(67)	9.12(66)	
	60	10.50(74)	10.65(75)	9.77(72)	6.65(51)	4.08(36)	5.17(42)	8.30(61)	10.63(74)	10.01(71)	
	75	9.23(64)	8.80(61)	8.46(59)	6.08(48)	3.90(33)	4.89(39)	7.49(54)	9.25(64)	9.20(63)	
	90	9.60(68)	10.29(72)	9.72(68)	8.43(61)	5.13(44)	6.06(47)	7.86(58)	9.83(69)	9.42(67)	
	105	8.24(56)	7.83(54)	8.12(56)	7.97(55)	6.33(46)	6.44(49)	7.33(51)	8.30(56)	8.81(59)	
	120	7.39(51)	6.56(46)	7.19(49)	7.35(50)	5.96(43)	6.65(47)	7.32(53)	7.17(49)	8.52(57)	
	135	9.51(61)	6.39(45)	6.24(44)	8.13(54)	7.30(49)	6.76(47)	7.16(49)	7.36(52)	9.80(62)	
	150	10.24(67)	6.58(47)	7.20(50)	9.31(62)	7.95(54)	7.68(53)	7.23(51)	7.52(52)	10.25(69)	
7.76–7.94	30	9.93(72)	10.14(70)	8.45(61)	5.86(46)	4.02(35)	4.65(39)	7.70(56)	9.84(68)	8.99(64)	
	45	9.33(66)	8.33(62)	7.20(53)	5.87(46)	4.26(36)	4.76(39)	6.91(52)	8.08(59)	8.60(62)	
	60	8.90(66)	7.90(60)	7.42(59)	5.68(46)	4.71(40)	4.98(42)	6.50(51)	7.82(59)	7.43(57)	
	75	7.52(55)	6.61(49)	6.29(47)	5.43(44)	4.41(36)	4.62(38)	6.05(46)	6.65(49)	6.97(51)	
	90	8.91(61)	8.54(59)	8.92(61)	8.72(60)	6.48(49)	7.03(50)	7.79(55)	8.17(57)	8.92(61)	
	105	9.09(59)	7.66(51)	7.81(52)	9.10(59)	7.99(53)	6.82(49)	7.78(52)	7.68(51)	8.87(58)	
	120	8.73(56)	6.36(44)	6.77(46)	8.68(55)	7.41(49)	7.55(50)	7.49(52)	6.91(46)	9.45(59)	
	135	9.31(57)	5.97(40)	6.18(42)	7.99(50)	7.69(49)	6.96(45)	6.58(43)	6.94(48)	8.93(55)	

Continued on next page

TABLE I – *Continued from previous page*

E_α	θ_n (deg)	Laboratory γ -Detection Angle (deg)									
		30	45	60	75	90	105	120	135	150	
	150	11.19(71)	7.00(49)	7.03(49)	9.39(62)	8.16(55)	7.76(53)	7.29(50)	7.50(52)	10.78(71)	
7.94–8.13	30	13.45(88)	14.83(92)	11.27(73)	6.56(49)	4.36(37)	6.45(48)	11.99(77)	13.53(85)	12.39(79)	
	45	12.84(79)	12.42(79)	9.79(64)	6.92(49)	4.60(37)	6.18(45)	10.83(69)	11.98(74)	10.68(68)	
	60	11.26(76)	9.86(68)	8.79(64)	5.78(45)	4.42(37)	5.88(46)	8.49(60)	10.27(70)	9.05(64)	
	75	7.84(60)	7.15(55)	5.81(47)	4.95(43)	4.03(36)	4.70(40)	6.33(50)	6.71(52)	7.00(54)	
	90	7.83(57)	7.45(54)	7.40(54)	7.33(53)	5.87(47)	6.74(50)	7.38(54)	7.54(55)	8.54(61)	
	105	9.82(64)	8.36(56)	7.70(52)	9.80(63)	8.64(57)	7.00(51)	8.72(58)	7.54(51)	9.89(64)	
	120	11.02(64)	7.18(46)	7.80(49)	9.47(57)	8.69(53)	8.32(51)	7.76(51)	7.82(49)	10.76(63)	
	135	12.68(69)	8.52(51)	8.36(50)	10.33(59)	9.68(56)	9.19(54)	8.38(50)	8.60(53)	12.03(66)	
	150	14.87(82)	10.68(62)	9.91(59)	11.81(68)	10.43(61)	9.84(59)	9.82(59)	10.28(61)	14.68(84)	
8.13–8.32	30	14.36(88)	14.35(85)	11.47(71)	7.22(50)	5.12(39)	7.20(50)	12.59(76)	13.52(81)	12.22(75)	
	45	14.60(82)	14.12(82)	11.28(66)	7.86(51)	5.45(39)	7.29(48)	12.02(70)	13.94(78)	12.35(71)	
	60	12.46(76)	11.30(70)	9.82(65)	6.24(44)	4.33(34)	6.48(46)	9.73(62)	11.50(71)	10.20(64)	
	75	7.17(52)	6.92(51)	5.14(40)	4.03(36)	2.68(26)	3.84(33)	5.90(45)	6.74(50)	6.53(49)	
	90	5.76(50)	6.05(52)	5.53(49)	4.76(43)	3.47(35)	4.49(41)	5.65(50)	5.97(52)	5.99(52)	
	105	6.85(52)	5.91(46)	5.73(45)	6.53(50)	5.78(45)	5.15(43)	6.55(50)	6.05(47)	7.43(56)	
	120	9.55(61)	7.19(49)	7.44(50)	8.08(54)	7.28(49)	7.32(50)	7.46(53)	7.45(50)	8.96(58)	
	135	13.29(72)	10.01(58)	8.44(51)	9.70(56)	8.62(51)	8.80(52)	9.84(57)	10.33(62)	12.61(70)	
	150	16.31(88)	13.37(74)	11.57(66)	11.26(65)	9.63(57)	9.74(58)	11.82(67)	12.85(72)	15.54(87)	
8.32–8.51	30	13.77(92)	11.31(76)	9.89(68)	7.75(57)	5.97(47)	6.42(49)	9.51(66)	11.53(77)	11.04(75)	
	45	12.11(76)	10.89(72)	9.31(61)	7.60(52)	5.57(42)	6.91(49)	8.83(59)	11.02(70)	11.39(72)	
	60	9.49(67)	8.98(64)	7.84(59)	5.38(43)	4.08(35)	5.28(42)	7.63(56)	8.56(61)	8.10(59)	
	75	5.58(48)	5.38(47)	4.11(38)	3.30(34)	2.01(23)	2.92(29)	4.74(42)	5.13(45)	4.90(43)	
	90	4.43(48)	4.61(50)	4.07(45)	2.74(33)	1.92(26)	2.72(32)	3.61(41)	4.40(48)	3.50(40)	
	105	3.95(39)	3.66(37)	3.86(38)	3.39(35)	2.89(31)	3.18(34)	4.12(40)	3.82(38)	4.22(41)	
	120	5.58(45)	5.14(42)	4.98(41)	4.78(40)	4.03(35)	4.56(39)	5.24(45)	5.49(45)	4.82(40)	
	135	9.49(62)	8.51(56)	7.28(50)	6.15(44)	4.73(36)	6.00(43)	8.51(56)	9.33(63)	8.57(57)	
	150	12.34(82)	11.46(77)	9.34(65)	6.78(50)	5.33(41)	6.37(47)	10.11(69)	11.18(75)	11.28(78)	
8.51–8.71	30	12.62(85)	11.00(73)	9.30(64)	7.23(53)	5.32(42)	5.88(46)	8.17(58)	11.06(73)	11.24(75)	
	45	9.36(64)	8.93(63)	7.75(55)	6.40(47)	4.31(36)	5.39(42)	6.74(49)	7.90(55)	9.27(63)	
	60	7.40(60)	6.82(56)	6.48(55)	4.06(37)	3.13(31)	3.66(35)	5.65(48)	6.23(52)	6.27(52)	
	75	3.84(38)	4.14(41)	3.70(37)	2.40(28)	1.43(19)	2.09(24)	3.40(35)	3.73(38)	3.42(35)	
	90	3.71(39)	4.10(43)	3.65(39)	2.48(29)	1.66(22)	1.98(24)	3.06(34)	3.86(40)	3.31(36)	
	105	3.44(35)	3.60(36)	3.47(35)	3.29(34)	2.30(26)	2.74(31)	3.74(37)	3.17(33)	3.52(35)	
	120	4.69(41)	4.59(40)	4.13(37)	3.99(36)	3.38(32)	3.68(34)	4.31(40)	4.79(41)	4.88(42)	
	135	7.08(51)	6.82(50)	6.14(46)	4.52(36)	3.34(29)	4.31(35)	6.43(47)	6.87(52)	6.22(46)	
	150	9.64(67)	9.95(68)	7.89(57)	4.93(39)	3.57(31)	4.92(39)	8.27(59)	9.49(66)	8.49(62)	
8.71–8.91	30	11.40(78)	11.19(74)	9.64(66)	6.90(51)	4.46(37)	5.85(45)	8.22(58)	10.37(70)	10.90(73)	
	45	8.94(61)	8.86(62)	7.83(54)	5.97(45)	3.74(32)	4.54(37)	6.56(48)	7.39(52)	7.81(55)	
	60	6.80(55)	5.84(49)	6.14(53)	3.77(35)	2.55(27)	3.02(30)	4.88(43)	5.50(47)	5.17(45)	
	75	3.59(37)	4.10(40)	3.82(38)	2.29(28)	1.33(18)	1.97(23)	3.02(32)	3.93(39)	3.15(33)	
	90	3.48(37)	4.03(41)	4.24(43)	3.06(33)	1.82(24)	2.05(25)	3.40(36)	3.73(39)	3.47(37)	
	105	3.59(35)	3.61(35)	3.65(35)	3.21(32)	2.58(27)	2.50(28)	3.46(34)	3.08(31)	3.28(32)	
	120	4.32(38)	4.25(37)	3.73(34)	3.71(34)	3.00(29)	3.51(32)	3.94(37)	4.21(37)	4.90(42)	
	135	6.43(47)	6.21(45)	4.96(38)	3.61(31)	3.38(29)	3.99(33)	5.78(43)	5.96(46)	5.92(44)	
	150	8.72(60)	8.83(61)	7.31(52)	4.56(37)	3.09(28)	4.48(36)	7.58(54)	8.52(59)	7.75(57)	
	30	11.08(77)	10.83(72)	10.44(70)	6.91(51)	3.73(33)	5.23(42)	8.38(59)	10.66(71)	11.06(74)	

Continued on next page

TABLE I – *Continued from previous page*

		Laboratory γ -Detection Angle (deg)									
		30	45	60	75	90	105	120	135	150	
E_α	θ_n (deg)										
8.91–9.12	45	8.34(59)	8.71(64)	7.86(56)	5.76(45)	3.53(32)	3.98(34)	6.72(50)	7.84(56)	7.24(53)	
	60	6.12(52)	5.72(49)	5.58(50)	3.81(36)	2.30(25)	2.53(27)	4.76(43)	5.30(46)	5.10(45)	
	75	3.79(40)	3.93(41)	3.66(38)	2.42(29)	1.43(19)	2.04(25)	3.10(34)	3.70(39)	3.19(35)	
	90	3.55(38)	4.05(42)	4.11(43)	3.39(37)	2.15(27)	2.31(27)	3.26(35)	3.80(40)	3.63(39)	
	105	4.10(38)	4.22(39)	4.58(42)	3.82(36)	3.12(31)	2.96(32)	3.94(37)	3.66(35)	4.42(41)	
	120	5.04(41)	4.45(37)	4.23(36)	4.50(37)	3.08(28)	3.80(33)	4.41(38)	4.70(39)	4.60(38)	
	135	6.19(45)	6.24(45)	4.86(38)	3.71(31)	3.33(29)	4.30(34)	5.63(42)	6.24(47)	6.29(46)	
	150	8.27(57)	8.16(57)	7.17(51)	4.62(37)	2.91(27)	4.35(35)	7.53(53)	8.35(58)	7.47(55)	
9.12–9.33	30	11.04(76)	11.10(73)	10.62(71)	6.84(51)	3.25(30)	4.47(38)	8.54(60)	11.28(74)	11.10(74)	
	45	7.22(53)	8.31(62)	6.63(50)	5.13(41)	3.01(28)	3.53(31)	5.97(46)	7.09(52)	6.79(51)	
	60	5.24(47)	5.71(50)	5.34(49)	3.41(33)	2.26(25)	2.43(26)	4.46(41)	5.13(46)	4.97(45)	
	75	4.12(42)	4.47(44)	4.07(41)	2.59(31)	1.29(18)	2.29(27)	3.39(36)	3.49(36)	3.50(37)	
	90	3.44(38)	3.95(42)	3.65(39)	2.98(33)	2.08(27)	2.33(28)	3.01(34)	3.79(41)	3.78(41)	
	105	3.69(36)	3.69(36)	3.99(38)	3.48(34)	2.47(27)	2.84(31)	3.52(35)	3.94(38)	4.28(41)	
	120	4.74(39)	4.27(36)	4.31(36)	4.46(37)	3.03(28)	3.47(31)	4.09(37)	4.61(38)	4.21(36)	
	135	5.93(44)	5.73(42)	4.84(37)	4.46(35)	3.27(28)	4.62(36)	5.61(42)	5.88(45)	6.19(45)	
	150	7.78(54)	7.24(51)	6.62(48)	4.91(38)	3.17(28)	4.47(36)	7.17(51)	7.98(55)	7.51(55)	
9.33–9.55	30	13.08(86)	14.46(90)	12.34(79)	7.50(54)	3.51(32)	4.99(40)	10.40(69)	14.18(88)	12.63(81)	
	45	9.15(62)	10.04(69)	7.97(56)	6.45(48)	3.31(30)	4.41(37)	7.03(51)	8.49(58)	8.62(60)	
	60	4.85(43)	5.55(48)	5.81(51)	3.56(34)	2.53(26)	2.56(27)	4.35(39)	5.37(47)	4.66(42)	
	75	3.34(35)	4.25(42)	3.86(39)	2.50(30)	1.42(19)	1.90(23)	3.09(33)	3.13(33)	3.25(34)	
	90	3.67(42)	4.11(46)	3.54(40)	2.66(32)	1.79(25)	2.02(26)	3.29(38)	3.47(40)	3.37(39)	
	105	3.35(35)	3.35(35)	3.34(35)	2.99(32)	2.25(26)	2.46(29)	3.05(32)	3.71(38)	3.86(39)	
	120	4.35(39)	3.98(36)	4.32(38)	3.92(36)	3.12(30)	3.42(32)	3.59(35)	4.47(39)	4.22(38)	
	135	5.16(40)	5.38(41)	4.80(38)	4.91(39)	3.76(32)	4.52(36)	5.68(43)	5.28(43)	5.83(44)	
	150	6.59(47)	5.76(42)	5.37(40)	4.79(37)	3.50(30)	4.33(34)	5.97(44)	7.01(49)	6.88(51)	
9.55–9.77	30	16.79(102)	18.82(108)	15.93(94)	8.84(59)	4.06(34)	6.25(46)	13.97(84)	19.87(113)	16.61(98)	
	45	11.46(71)	12.21(77)	10.96(68)	7.93(53)	4.00(33)	5.00(39)	9.25(60)	12.03(73)	10.99(69)	
	60	6.42(51)	6.94(54)	6.59(53)	4.80(40)	2.91(28)	3.16(30)	5.53(45)	6.65(52)	5.79(47)	
	75	3.41(35)	3.79(38)	3.79(39)	2.49(29)	1.96(23)	1.79(22)	3.12(33)	3.38(35)	3.37(35)	
	90	3.58(38)	3.59(38)	3.12(34)	2.65(30)	1.63(22)	1.82(23)	2.89(32)	3.12(34)	3.00(33)	
	105	3.09(33)	3.11(33)	3.03(33)	3.02(33)	1.99(24)	2.17(27)	2.62(29)	2.95(32)	3.65(38)	
	120	3.69(35)	3.23(32)	3.77(36)	3.43(33)	3.01(30)	2.97(30)	3.06(32)	3.70(35)	3.66(35)	
	135	4.25(37)	4.31(37)	4.27(37)	4.48(38)	3.75(33)	3.73(33)	4.52(38)	4.58(41)	4.94(41)	
	150	5.42(42)	4.53(37)	4.16(35)	4.36(36)	3.77(32)	3.92(33)	4.63(37)	5.57(43)	5.59(45)	
9.77–10.00	30	18.35(110)	22.49(126)	18.11(105)	9.54(63)	3.70(33)	7.05(51)	16.30(96)	22.46(126)	18.67(108)	
	45	11.30(69)	12.00(74)	11.17(67)	7.32(49)	3.79(31)	4.76(36)	9.07(58)	12.33(73)	11.38(69)	
	60	7.48(56)	8.27(60)	6.86(54)	5.26(42)	3.20(30)	3.75(33)	6.19(48)	7.34(55)	7.23(54)	
	75	4.32(41)	4.36(41)	4.17(40)	2.93(32)	2.39(26)	2.14(24)	3.70(36)	4.20(40)	4.10(39)	
	90	4.27(45)	4.23(44)	3.83(41)	3.33(37)	2.00(26)	2.22(27)	3.34(37)	3.95(42)	3.97(42)	
	105	3.02(33)	2.77(31)	2.97(33)	2.88(32)	1.94(24)	2.00(25)	2.35(27)	2.43(28)	3.00(33)	
	120	3.17(34)	2.66(29)	3.04(33)	3.26(34)	2.71(30)	2.25(26)	2.60(30)	2.90(31)	3.21(34)	
	135	3.73(36)	3.05(31)	3.33(33)	3.51(35)	3.01(31)	3.08(31)	3.13(32)	3.64(37)	4.04(39)	
	150	4.68(43)	3.51(34)	3.14(31)	3.64(35)	3.17(31)	3.15(31)	3.59(35)	3.84(36)	4.42(42)	
10.00–10.23	30	13.56(87)	18.22(107)	13.79(85)	7.31(52)	2.83(27)	5.37(42)	12.63(79)	16.49(99)	14.05(87)	
	45	10.92(69)	10.94(71)	10.11(64)	6.60(47)	3.43(30)	4.23(34)	8.41(56)	10.93(68)	10.90(68)	
	60	7.10(55)	7.82(59)	6.60(54)	4.94(41)	3.40(32)	3.67(33)	5.72(46)	6.92(54)	7.55(58)	
	75	4.11(39)	4.11(39)	3.75(36)	2.96(32)	2.19(24)	2.22(25)	3.60(35)	4.01(38)	4.03(39)	
	90	3.94(42)	4.17(44)	3.61(39)	3.28(36)	2.28(29)	2.37(28)	3.08(34)	3.55(38)	3.65(39)	

Continued on next page

TABLE I – *Continued from previous page*

		Laboratory γ -Detection Angle (deg)									
E_α		30	45	60	75	90	105	120	135	150	
10.23–10.47	105	3.04(34)	2.72(31)	2.74(31)	2.66(30)	2.32(27)	1.95(25)	2.35(27)	2.49(29)	2.39(28)	
	120	2.41(27)	2.04(24)	2.16(25)	2.51(28)	2.02(24)	1.75(21)	1.82(23)	1.94(23)	2.25(26)	
	135	2.95(30)	2.49(27)	2.51(27)	2.55(27)	2.30(25)	2.50(27)	2.51(27)	2.75(30)	3.40(34)	
	150	3.62(35)	2.93(30)	2.59(27)	2.94(30)	2.14(24)	2.62(27)	2.74(28)	3.30(33)	3.92(39)	
10.47–10.72	30	12.47(86)	15.17(97)	11.18(76)	6.87(52)	3.19(31)	4.39(38)	11.02(75)	14.06(91)	12.51(83)	
	45	10.40(70)	10.02(70)	9.25(64)	6.29(48)	3.47(32)	3.72(33)	7.50(54)	9.37(64)	10.10(69)	
	60	6.15(53)	6.47(55)	5.46(50)	4.37(40)	2.96(30)	3.19(32)	4.78(43)	5.79(50)	6.59(56)	
	75	4.15(42)	3.87(39)	3.63(37)	3.33(37)	1.99(24)	2.35(27)	3.18(34)	3.81(39)	3.84(39)	
	90	2.91(31)	2.69(29)	2.78(30)	2.54(28)	2.14(25)	1.88(22)	2.21(25)	2.38(26)	2.91(31)	
	105	2.68(29)	2.21(25)	2.39(27)	2.76(30)	2.16(25)	2.02(25)	2.17(25)	2.23(25)	2.33(26)	
	120	3.40(34)	2.45(27)	2.50(27)	3.08(32)	2.87(30)	2.43(26)	2.10(25)	2.18(24)	2.82(30)	
	135	3.79(36)	3.20(31)	2.78(28)	2.88(29)	2.68(27)	3.13(31)	3.34(32)	3.09(32)	4.02(37)	
	150	4.20(37)	3.19(30)	3.00(28)	3.03(29)	2.26(23)	3.02(29)	3.22(30)	3.87(34)	4.16(38)	
	30	13.02(89)	14.56(94)	11.79(79)	6.87(52)	2.98(29)	4.36(37)	11.31(76)	14.39(93)	12.41(83)	
10.72–10.96	45	9.82(69)	9.58(69)	8.67(62)	5.80(46)	3.40(31)	3.87(34)	6.86(52)	9.25(65)	9.81(69)	
	60	5.52(51)	5.51(51)	4.64(46)	4.04(40)	2.59(29)	2.72(30)	4.20(41)	5.43(50)	5.95(54)	
	75	3.32(36)	3.35(37)	3.28(36)	3.12(36)	1.56(21)	1.96(24)	2.38(28)	3.23(36)	3.06(34)	
	90	3.18(34)	3.08(33)	3.60(38)	3.07(33)	2.68(31)	2.28(27)	2.76(31)	3.15(34)	3.79(39)	
	105	3.20(33)	2.48(27)	3.00(31)	3.36(34)	2.69(29)	2.53(29)	2.63(28)	2.41(27)	3.00(32)	
	120	3.54(33)	2.52(26)	2.49(25)	3.17(30)	3.02(29)	2.76(27)	2.45(26)	2.60(26)	3.24(31)	
	135	4.32(37)	3.50(31)	2.93(27)	2.98(28)	3.11(29)	3.58(32)	3.65(32)	3.11(30)	3.88(34)	
	150	5.14(41)	3.94(34)	3.59(31)	3.01(28)	2.61(25)	3.30(30)	4.45(37)	4.64(38)	4.55(39)	
	30	14.70(97)	16.49(103)	14.82(94)	6.93(52)	2.77(28)	5.26(42)	12.64(83)	16.33(102)	13.85(89)	
	45	10.25(69)	10.55(73)	9.84(66)	5.63(44)	3.22(30)	3.99(34)	7.66(55)	10.50(70)	9.78(66)	
10.96–11.22	60	6.11(55)	5.59(51)	4.80(47)	4.08(40)	2.60(29)	2.68(29)	4.49(43)	5.91(53)	5.81(52)	
	75	2.79(32)	2.77(31)	2.78(31)	2.33(29)	1.36(18)	1.67(21)	2.23(26)	2.56(29)	2.40(28)	
	90	2.73(32)	2.81(32)	2.84(33)	2.81(32)	2.07(27)	2.13(26)	2.40(29)	2.82(33)	2.57(30)	
	105	3.08(33)	2.66(29)	2.86(31)	3.06(32)	2.77(30)	2.35(28)	2.55(28)	2.50(28)	3.12(33)	
	120	3.17(30)	2.33(24)	2.41(25)	2.94(29)	2.63(26)	2.50(25)	2.47(26)	2.73(27)	2.88(28)	
	135	4.08(35)	3.48(31)	2.86(27)	2.69(26)	2.75(26)	3.08(29)	3.55(32)	3.05(30)	3.55(32)	
	150	5.16(43)	4.86(41)	3.86(34)	2.44(24)	2.38(24)	3.05(29)	4.72(40)	4.92(41)	4.51(40)	
	30	14.01(94)	16.30(103)	14.18(91)	6.54(50)	2.64(27)	5.48(44)	11.73(78)	15.33(98)	13.93(91)	
	45	10.09(68)	11.27(76)	10.22(68)	6.00(46)	3.13(29)	4.20(36)	7.98(56)	10.43(69)	9.48(64)	
	60	5.64(51)	5.22(48)	4.67(46)	3.39(34)	2.42(27)	2.69(29)	4.40(42)	5.19(48)	5.09(47)	
11.22–11.48	75	2.84(33)	2.96(35)	2.43(30)	2.00(27)	1.40(20)	1.85(24)	2.49(30)	2.55(31)	2.22(28)	
	90	3.01(37)	2.78(34)	2.92(36)	2.80(35)	1.81(26)	2.11(28)	2.64(33)	2.99(36)	2.22(29)	
	105	2.21(27)	2.39(29)	2.25(27)	2.54(30)	2.24(27)	2.08(27)	2.11(26)	2.26(27)	2.83(33)	
	120	2.93(30)	2.06(23)	2.10(24)	2.45(26)	2.10(24)	2.13(24)	2.35(27)	2.46(27)	2.36(26)	
	135	3.75(35)	3.44(33)	2.94(29)	2.32(25)	1.84(21)	2.40(25)	3.56(34)	3.24(33)	3.43(33)	
	150	5.27(45)	5.03(44)	3.87(35)	2.21(23)	1.77(20)	2.68(27)	4.31(39)	5.31(46)	4.63(42)	
	30	12.13(87)	14.17(96)	11.54(81)	6.16(49)	2.57(27)	4.97(42)	9.88(71)	13.30(91)	12.13(85)	
	45	8.25(60)	9.25(68)	7.77(57)	5.05(41)	2.96(28)	3.55(32)	6.69(51)	8.27(60)	8.06(59)	
	60	4.66(46)	4.74(46)	4.14(43)	2.90(31)	2.23(26)	2.34(27)	3.67(38)	4.41(44)	4.32(43)	
	75	2.86(35)	3.19(38)	2.46(31)	1.92(27)	1.31(20)	1.89(26)	2.52(32)	2.48(32)	2.43(31)	

Continued on next page

TABLE I – *Continued from previous page*

E_α	θ_n (deg)	Laboratory γ -Detection Angle (deg)								
		30	45	60	75	90	105	120	135	150
11.48–11.75	30	11.05(83)	12.88(92)	10.25(76)	5.84(48)	2.67(28)	4.61(41)	8.71(66)	12.20(88)	11.08(81)
	45	8.08(61)	8.33(65)	7.25(56)	4.90(41)	3.07(30)	3.74(34)	5.97(48)	7.52(57)	7.75(59)
	60	4.59(46)	4.59(46)	3.80(42)	3.12(34)	2.41(28)	1.99(25)	3.10(34)	3.86(40)	4.25(44)
	75	2.10(28)	2.14(28)	1.94(26)	1.43(22)	1.12(18)	1.16(18)	1.71(24)	1.83(25)	2.15(29)
	90	1.90(29)	1.95(30)	2.20(33)	1.98(30)	1.53(26)	1.54(25)	1.99(31)	1.91(29)	2.26(34)
	105	1.59(24)	1.86(27)	1.54(23)	1.87(27)	1.43(22)	1.66(26)	1.95(28)	2.13(30)	2.03(29)
	120	2.71(33)	2.15(27)	1.70(23)	1.71(23)	1.65(22)	1.63(22)	1.79(25)	2.13(27)	2.41(30)
	135	2.74(30)	2.67(30)	2.19(25)	1.43(19)	1.28(17)	1.75(21)	2.77(31)	3.00(34)	2.39(27)
	150	4.07(40)	4.24(42)	3.35(35)	1.57(20)	1.30(17)	2.18(25)	3.99(40)	4.06(40)	3.27(35)
11.75–12.02	30	10.80(84)	12.15(90)	9.69(74)	5.51(48)	2.93(30)	4.06(38)	8.16(65)	11.61(86)	10.37(79)
	45	7.25(56)	7.04(56)	6.61(52)	4.64(40)	2.64(27)	3.49(32)	5.25(43)	7.16(55)	6.53(52)
	60	3.82(41)	3.61(39)	3.50(40)	2.89(33)	2.08(26)	1.79(23)	2.79(32)	3.44(38)	3.55(39)
	75	2.28(33)	1.87(28)	1.74(26)	1.48(24)	1.12(19)	0.90(16)	1.52(24)	1.93(29)	2.03(30)
	90	1.64(29)	1.92(33)	2.05(35)	1.82(32)	1.29(25)	1.45(26)	1.84(32)	1.87(32)	1.68(30)
	105	1.73(27)	1.60(25)	1.44(23)	1.97(30)	1.20(20)	1.27(22)	1.97(30)	1.94(29)	1.63(26)
	120	1.94(26)	1.73(23)	1.43(20)	1.39(20)	1.19(17)	1.43(20)	1.45(21)	1.57(22)	1.87(25)
	135	2.75(33)	2.39(29)	1.98(26)	1.55(21)	1.57(21)	2.13(27)	2.49(30)	3.15(38)	2.40(30)
	150	3.30(37)	3.20(36)	2.70(32)	1.55(21)	1.24(18)	1.81(23)	3.17(36)	3.36(38)	2.82(34)
12.02–12.30	30	9.65(77)	10.86(82)	9.43(73)	4.87(44)	2.45(27)	3.46(34)	7.45(60)	10.66(81)	9.37(73)
	45	7.10(59)	6.66(58)	6.01(51)	4.28(40)	2.47(27)	2.71(29)	5.04(45)	7.48(61)	6.38(54)
	60	3.39(39)	3.64(41)	3.11(38)	2.51(31)	1.74(23)	1.68(23)	2.62(32)	3.15(37)	2.83(34)
	75	1.95(29)	1.69(26)	1.54(24)	1.36(23)	0.97(17)	0.92(16)	1.57(24)	1.54(24)	1.61(25)
	90	1.52(25)	1.54(25)	1.52(25)	1.43(24)	1.17(21)	0.96(17)	1.38(23)	1.21(21)	1.39(23)
	105	1.84(29)	1.46(24)	1.24(21)	1.78(28)	1.05(18)	1.06(20)	1.67(26)	1.77(28)	1.43(23)
	120	1.90(26)	1.90(26)	1.63(23)	1.63(23)	1.42(21)	1.47(21)	1.60(24)	1.56(22)	1.70(24)
	135	2.56(30)	2.15(26)	1.73(22)	1.65(21)	1.51(20)	2.04(25)	2.44(29)	2.77(33)	2.60(30)
	150	3.60(40)	2.93(34)	2.70(32)	1.76(23)	1.58(21)	2.09(26)	3.07(35)	3.52(40)	3.19(38)
12.30–12.59	30	7.96(69)	8.48(70)	7.77(65)	3.76(37)	1.67(21)	2.75(30)	5.67(50)	8.14(68)	7.40(63)
	45	6.06(54)	5.95(55)	4.93(45)	3.74(37)	2.21(26)	1.95(23)	4.17(40)	5.84(52)	5.67(51)
	60	3.34(41)	3.29(40)	2.45(33)	2.39(31)	1.70(24)	1.57(23)	2.46(32)	2.55(33)	2.68(34)
	75	1.70(28)	1.51(25)	1.54(25)	1.24(22)	0.85(16)	1.00(18)	1.44(24)	1.24(21)	1.46(24)
	90	1.24(23)	1.05(20)	1.15(22)	1.10(21)	0.99(20)	0.85(17)	0.88(17)	1.04(20)	1.19(22)
	105	1.71(28)	1.56(26)	1.24(22)	1.54(26)	1.36(23)	1.01(19)	1.44(24)	1.44(24)	1.69(28)
	120	1.68(23)	1.66(23)	1.55(22)	1.61(22)	1.39(20)	1.26(19)	1.45(22)	1.28(19)	1.58(22)
	135	2.33(28)	2.11(26)	1.69(22)	1.82(23)	1.46(19)	1.83(23)	2.45(29)	2.23(28)	2.47(29)
	150	3.69(39)	2.82(32)	2.52(29)	1.71(22)	1.63(21)	2.03(24)	2.74(31)	3.19(35)	3.22(36)
12.59–12.88	30	8.56(75)	8.37(71)	7.54(66)	3.87(39)	1.65(22)	2.63(30)	5.73(53)	8.49(72)	7.49(66)
	45	5.51(50)	5.86(54)	5.21(48)	3.32(34)	2.17(25)	2.05(24)	4.19(40)	5.18(48)	4.94(46)
	60	3.21(40)	2.76(36)	2.55(35)	2.30(31)	1.53(23)	1.64(24)	2.30(31)	2.72(35)	2.59(34)
	75	1.37(24)	1.24(22)	1.17(21)	0.90(18)	0.66(14)	0.86(17)	0.94(18)	0.92(18)	1.21(22)
	90	1.14(23)	1.23(25)	1.39(27)	1.37(27)	1.17(24)	1.25(25)	1.10(22)	1.31(26)	1.11(23)
	105	1.56(27)	1.51(26)	1.40(24)	1.44(25)	1.46(25)	0.89(18)	1.26(22)	1.19(21)	1.55(26)
	120	1.83(26)	1.40(21)	1.52(22)	1.75(25)	1.56(23)	1.45(21)	1.39(22)	1.37(20)	1.80(25)
	135	2.27(27)	1.67(21)	1.30(18)	1.66(21)	1.41(19)	1.65(21)	1.77(22)	1.94(25)	1.78(23)
	150	3.13(35)	2.40(28)	1.96(24)	1.53(20)	1.32(18)	1.57(20)	2.20(26)	2.57(30)	2.56(31)
	30	7.50(67)	7.65(66)	6.84(60)	3.94(39)	1.51(20)	2.30(26)	5.68(52)	7.79(67)	7.24(63)
	45	5.42(49)	5.36(50)	4.58(43)	3.11(32)	1.61(21)	2.07(24)	3.70(37)	5.14(47)	4.54(43)

Continued on next page

TABLE I – *Continued from previous page*

		Laboratory γ -Detection Angle (deg)									
		30	45	60	75	90	105	120	135	150	
E_α		60	2.50(33)	2.43(32)	2.10(29)	1.68(24)	1.04(17)	1.19(18)	1.62(23)	2.19(29)	2.02(27)
12.88–13.18	75	1.18(25)	1.17(25)	0.89(20)	0.84(19)	0.72(16)	0.77(17)	0.81(18)	0.91(20)	0.98(21)	
	90	1.10(21)	1.07(20)	1.09(21)	1.29(24)	0.69(15)	0.87(17)	0.89(18)	0.85(17)	0.75(16)	
	105	1.31(23)	1.40(24)	1.29(23)	1.37(24)	1.28(22)	1.11(21)	1.30(23)	1.15(21)	1.20(21)	
	120	1.34(20)	0.85(14)	1.21(18)	1.32(19)	1.09(17)	1.11(17)	1.05(17)	1.00(16)	1.35(20)	
	135	2.26(27)	1.47(20)	1.04(15)	1.47(20)	1.17(17)	1.36(18)	1.49(20)	1.80(24)	1.56(20)	
	150	2.51(29)	2.26(27)	1.75(22)	1.51(20)	1.18(17)	1.50(20)	2.07(25)	2.48(29)	2.05(26)	
13.18–13.49	30	7.18(68)	7.72(70)	6.10(58)	3.55(37)	1.58(21)	2.10(25)	5.21(51)	7.01(65)	7.29(67)	
	45	5.86(54)	5.30(51)	4.60(44)	3.57(37)	1.73(22)	2.16(26)	3.67(37)	5.10(48)	4.91(47)	
	60	2.70(39)	2.77(40)	2.35(36)	1.86(29)	1.48(24)	1.21(21)	1.89(29)	2.14(32)	2.57(38)	
	75	1.50(26)	1.16(21)	1.19(22)	0.96(19)	0.73(15)	0.88(17)	0.91(18)	0.99(19)	1.06(20)	
	90	1.40(25)	1.13(21)	1.40(25)	1.18(21)	0.58(13)	0.80(16)	0.73(15)	0.81(16)	0.89(17)	
	105	0.87(16)	1.19(21)	0.95(17)	0.97(18)	0.89(16)	0.86(17)	1.02(18)	0.89(16)	0.97(18)	
	120	1.36(21)	1.02(17)	1.47(22)	1.18(19)	1.01(17)	1.09(18)	1.11(19)	0.91(15)	1.37(21)	
	135	1.80(24)	1.33(19)	1.18(17)	1.33(19)	1.01(15)	1.22(18)	1.42(20)	1.63(23)	1.47(20)	
	150	2.08(26)	1.97(25)	1.77(23)	1.48(20)	1.06(16)	1.41(19)	2.13(26)	2.38(29)	2.04(27)	
13.49–13.80	30	6.61(67)	7.18(69)	5.70(57)	3.07(35)	1.34(20)	2.05(26)	4.37(46)	6.23(62)	6.33(63)	
	45	4.94(49)	4.71(48)	4.28(43)	2.99(33)	1.81(23)	1.88(23)	3.55(37)	4.23(43)	4.51(45)	
	60	2.63(35)	2.53(34)	2.25(32)	1.83(26)	1.27(20)	1.24(20)	1.61(24)	1.85(26)	2.33(32)	
	75	1.68(32)	1.08(22)	1.22(24)	0.95(21)	0.80(18)	1.13(23)	0.97(20)	0.81(18)	1.19(24)	
	90	1.18(23)	1.26(25)	1.54(29)	1.09(22)	0.70(16)	0.88(18)	0.68(15)	0.81(17)	0.94(19)	
	105	0.95(17)	1.02(18)	0.97(17)	0.78(14)	0.73(14)	0.67(14)	0.81(15)	0.74(14)	0.80(15)	
	120	1.26(21)	0.95(16)	1.21(20)	1.16(19)	0.99(17)	1.01(17)	0.90(17)	0.92(16)	0.92(16)	
	135	1.38(20)	1.29(19)	1.22(18)	1.08(17)	1.24(19)	1.33(19)	1.68(23)	1.62(24)	1.48(21)	
	150	2.23(28)	1.86(24)	1.44(20)	1.22(18)	0.89(14)	1.22(18)	2.00(26)	2.05(26)	1.93(26)	
13.80–14.13	30	6.33(68)	6.37(67)	5.74(61)	2.96(36)	1.29(20)	2.12(28)	3.98(45)	6.02(63)	5.23(56)	
	45	5.19(53)	5.21(55)	4.73(49)	2.86(33)	1.76(24)	2.02(26)	3.79(41)	4.41(46)	4.73(49)	
	60	3.01(39)	2.63(35)	2.56(35)	2.09(29)	1.08(18)	1.43(22)	1.72(25)	2.01(28)	2.40(33)	
	75	1.53(29)	1.00(21)	0.96(20)	0.90(20)	0.88(19)	0.92(19)	0.76(17)	0.85(18)	1.31(26)	
	90	0.89(18)	1.08(21)	1.17(23)	1.05(21)	0.56(13)	0.67(15)	0.65(14)	0.90(19)	0.88(18)	
	105	1.11(20)	0.90(17)	1.03(19)	0.88(17)	0.96(18)	0.91(18)	1.00(19)	0.79(16)	0.98(18)	
	120	1.39(21)	1.06(17)	1.16(18)	1.59(23)	1.22(19)	1.20(19)	1.04(18)	0.94(16)	1.08(17)	
	135	1.79(24)	1.63(23)	1.23(19)	1.17(18)	1.41(21)	1.38(20)	1.86(25)	1.87(26)	1.75(24)	
	150	2.58(32)	2.16(28)	1.52(21)	1.13(17)	0.92(15)	1.18(18)	2.15(28)	2.01(26)	1.97(27)	
14.13–14.45	30	6.40(70)	6.48(69)	5.76(62)	3.28(39)	1.70(24)	2.29(30)	4.70(53)	6.43(68)	5.28(58)	
	45	4.87(50)	4.68(49)	4.10(43)	2.56(30)	1.63(22)	2.06(26)	3.18(35)	3.98(42)	3.90(42)	
	60	2.56(37)	2.18(32)	2.32(35)	1.82(28)	1.01(18)	1.54(25)	1.50(24)	1.84(28)	2.02(31)	
	75	1.49(28)	1.07(21)	1.12(22)	0.95(20)	0.95(20)	0.83(18)	0.59(14)	1.11(22)	1.37(26)	
	90	0.84(19)	0.72(17)	0.83(19)	0.80(18)	0.39(11)	0.59(14)	0.51(12)	0.63(15)	0.72(17)	
	105	0.68(14)	0.80(16)	0.90(18)	0.76(16)	0.90(18)	0.71(15)	0.90(18)	0.82(17)	0.83(17)	
	120	0.95(17)	0.78(15)	0.88(16)	1.10(19)	0.86(16)	0.84(15)	0.78(15)	0.71(13)	0.97(17)	
	135	1.75(26)	1.71(25)	1.15(19)	1.24(20)	1.12(18)	1.23(20)	1.70(25)	1.92(29)	1.53(23)	
	150	2.29(30)	2.19(29)	1.68(24)	1.15(18)	0.85(14)	1.11(17)	2.22(29)	2.32(31)	2.07(29)	
14.45–14.79	30	5.65(62)	6.15(64)	5.00(54)	3.16(37)	1.61(23)	2.32(30)	4.09(46)	5.26(56)	4.84(53)	
	45	4.02(42)	4.08(44)	3.38(36)	2.50(29)	1.76(22)	1.88(23)	2.74(31)	3.30(36)	3.34(36)	
	60	2.14(31)	2.05(29)	1.94(29)	1.68(25)	1.07(18)	1.50(23)	1.22(20)	1.63(25)	1.62(24)	
	75	1.45(31)	1.03(23)	1.20(26)	0.89(22)	0.89(21)	0.95(22)	0.66(16)	0.98(22)	1.15(25)	
	90	0.85(20)	0.65(16)	0.63(16)	0.61(15)	0.45(13)	0.58(15)	0.35(10)	0.52(14)	0.55(14)	
	105	0.37(10)	0.57(13)	0.88(19)	0.76(17)	0.64(15)	0.52(13)	0.65(15)	0.65(15)	0.58(14)	

Continued on next page

TABLE I – *Continued from previous page*

		θ_n (deg)	Laboratory γ -Detection Angle (deg)								
		E_α	30	45	60	75	90	105	120	135	150
		120	1.00(20)	0.75(16)	0.97(19)	1.06(20)	0.88(18)	0.85(17)	0.72(16)	0.88(18)	0.93(18)
		135	1.69(27)	1.50(25)	1.15(20)	1.02(19)	0.93(17)	1.31(22)	1.60(26)	1.62(28)	1.29(22)
		150	2.04(29)	2.21(31)	1.61(24)	0.96(16)	0.78(14)	1.03(17)	1.98(28)	2.39(33)	1.72(27)
		30	5.54(64)	5.57(62)	4.59(53)	2.56(33)	1.44(22)	1.98(27)	3.13(39)	4.78(55)	4.81(55)
		45	4.13(44)	4.09(45)	3.94(42)	2.54(30)	1.95(25)	1.88(24)	3.05(34)	3.31(37)	3.45(38)
		60	2.72(39)	2.95(41)	2.57(38)	2.58(37)	1.60(26)	1.67(26)	1.92(30)	2.13(32)	2.53(37)
		75	1.15(25)	0.90(20)	1.00(22)	0.85(20)	0.68(16)	0.79(18)	0.65(16)	0.72(17)	1.14(25)
		90	0.86(20)	0.82(19)	0.80(19)	0.78(18)	0.53(14)	0.64(16)	0.62(15)	0.65(16)	0.40(11)
		105	0.40(11)	0.35(10)	0.76(18)	0.72(17)	0.42(11)	0.60(15)	0.56(14)	0.37(10)	0.70(17)
		120	0.73(16)	0.65(15)	0.65(15)	0.69(15)	0.67(15)	0.68(15)	0.65(15)	0.60(14)	0.62(14)
		135	1.42(25)	1.04(20)	0.83(17)	0.83(17)	0.59(13)	1.07(20)	0.88(17)	1.10(22)	0.94(18)
		150	2.15(39)	2.21(40)	1.73(32)	0.97(20)	0.84(18)	0.93(20)	1.94(36)	2.16(39)	1.78(34)
		30	5.27(63)	5.04(59)	4.19(50)	2.43(32)	1.48(22)	1.57(23)	3.27(41)	4.29(51)	4.48(53)
		45	3.89(44)	3.38(40)	3.66(42)	2.20(28)	1.44(20)	1.59(22)	2.47(31)	2.88(34)	3.01(36)
		60	2.14(34)	2.16(34)	1.63(28)	1.96(31)	1.20(21)	1.04(19)	1.32(23)	1.45(24)	2.06(33)
		75	0.87(19)	0.82(18)	0.77(17)	0.90(20)	0.60(14)	0.61(14)	0.43(11)	0.64(15)	0.99(21)
		90	1.01(28)	1.01(28)	1.11(30)	1.25(33)	0.90(26)	0.86(24)	1.21(32)	0.78(22)	0.81(23)
		105	0.47(12)	0.35(10)	0.77(19)	0.57(15)	0.42(11)	0.57(15)	0.59(15)	0.46(12)	0.62(16)
		120	0.46(12)	0.59(14)	0.66(16)	0.66(16)	0.67(16)	0.66(16)	0.69(17)	0.71(17)	0.70(17)
		135	1.35(25)	1.03(20)	0.83(17)	0.91(19)	0.68(15)	0.86(18)	1.10(22)	1.22(24)	1.06(21)
		150	1.33(22)	1.38(23)	1.14(20)	0.71(14)	0.55(11)	0.69(13)	1.40(23)	1.41(23)	1.34(23)
		30	4.99(62)	4.55(56)	3.87(49)	2.40(33)	1.29(21)	1.48(23)	3.25(42)	3.95(50)	3.64(47)
		45	4.02(49)	3.63(45)	3.68(45)	2.71(35)	1.45(22)	1.54(23)	2.18(30)	2.70(35)	3.23(41)
		60	1.98(32)	1.94(32)	1.72(29)	1.35(23)	1.11(20)	0.79(16)	1.13(20)	1.29(23)	1.83(30)
		75	0.90(20)	0.74(17)	0.78(17)	0.73(17)	0.48(12)	0.57(14)	0.45(11)	0.49(12)	0.85(19)
		90	0.63(18)	0.52(15)	0.48(14)	0.58(16)	0.42(13)	0.49(14)	0.60(17)	0.52(15)	0.65(18)
		105	0.64(17)	0.49(14)	0.85(21)	0.76(20)	0.72(19)	0.61(17)	0.71(19)	0.66(17)	0.74(19)
		120	0.41(11)	0.46(12)	0.46(12)	0.66(16)	0.59(15)	0.55(14)	0.61(16)	0.59(15)	0.73(18)
		135	0.81(16)	0.69(14)	0.76(15)	0.60(13)	0.55(12)	0.50(11)	0.75(15)	0.80(17)	0.81(16)
		150	0.94(18)	1.04(19)	0.69(14)	0.56(12)	0.50(11)	0.57(12)	0.95(18)	1.20(21)	0.97(19)
		30	5.00(69)	4.64(63)	3.80(53)	2.01(31)	1.23(22)	1.37(24)	3.16(45)	4.46(61)	3.52(50)
		45	3.93(48)	3.82(48)	3.28(41)	2.65(35)	1.42(22)	1.32(21)	2.23(30)	2.82(36)	3.18(40)
		60	1.70(30)	1.99(35)	2.28(40)	1.24(23)	1.22(23)	0.85(18)	1.53(28)	1.42(26)	1.77(32)
		75	1.07(28)	0.85(23)	1.07(28)	0.81(22)	0.53(15)	0.65(18)	0.67(19)	0.48(14)	0.95(25)
		90	0.79(23)	0.62(19)	0.57(17)	0.51(16)	0.42(14)	0.69(21)	0.66(20)	0.60(18)	0.74(22)
		105	0.60(17)	0.50(15)	0.42(13)	0.56(16)	0.43(13)	0.41(13)	0.31(10)	0.48(14)	0.52(15)
		120	0.49(13)	0.50(13)	0.32(9)	0.65(16)	0.42(11)	0.48(13)	0.61(16)	0.51(13)	0.59(15)
		135	0.68(16)	0.67(16)	0.75(17)	0.72(16)	0.56(14)	0.58(14)	0.64(15)	0.92(21)	0.85(19)
		150	0.99(19)	0.85(17)	0.29(8)	0.51(11)	0.60(13)	0.53(12)	0.78(16)	1.01(20)	1.01(20)
		30	3.89(54)	3.97(54)	3.08(43)	1.89(29)	0.97(18)	1.30(22)	2.44(36)	3.45(48)	3.16(45)
		45	3.36(46)	3.02(43)	2.41(34)	1.84(28)	1.16(20)	1.09(19)	2.05(30)	2.54(36)	2.47(35)
		60	1.48(27)	1.59(29)	1.71(32)	1.33(25)	1.02(20)	0.91(18)	1.50(28)	1.42(26)	1.34(25)
		75	0.75(20)	0.84(22)	0.86(22)	0.77(21)	0.56(16)	0.54(15)	0.58(16)	0.52(15)	0.60(17)
		90	0.57(17)	0.61(18)	0.78(22)	0.46(14)	0.49(15)	0.63(18)	0.64(18)	0.53(16)	0.56(16)
		105	0.74(21)	0.78(22)	0.49(15)	0.74(21)	0.44(13)	0.49(15)	0.53(16)	0.71(20)	0.54(16)
		120	0.41(12)	0.35(11)	0.47(14)	0.55(16)	0.55(16)	0.42(13)	0.57(17)	0.58(17)	0.59(17)
		135	0.62(16)	0.60(15)	0.60(15)	0.70(17)	0.57(15)	0.62(16)	0.54(14)	0.65(17)	0.75(18)
		150	0.96(21)	0.71(16)	0.34(9)	0.42(11)	0.54(13)	0.62(15)	0.76(17)	0.85(19)	0.98(22)

Continued on next page

TABLE I – *Continued from previous page*

E_α	θ_n (deg)	Laboratory γ -Detection Angle (deg)								
		30	45	60	75	90	105	120	135	150

TABLE II: The normalized n angular distributions measured in this work as a function of incident neutron energy, E_α , and laboratory n -detection angle. The uncertainty on all the laboratory n -detection angles is $\pm 5^\circ$. The overall scaling of the n distribution values is arbitrary.

E_α	Laboratory n -Detection Angle, θ_n (deg)								
	30	45	60	75	90	105	120	135	150
6.45–6.61	1.61(7)	1.88(8)	1.65(8)	1.10(7)	1.31(9)	1.75(10)	2.08(11)	2.83(14)	3.30(17)
6.61–6.76	1.62(9)	1.79(9)	1.34(8)	0.85(6)	0.99(8)	1.47(10)	1.64(10)	2.05(11)	2.20(13)
6.76–6.92	1.24(8)	1.57(8)	1.20(8)	0.70(6)	0.90(7)	1.23(9)	1.50(9)	1.75(10)	1.77(12)
6.92–7.08	1.49(9)	1.66(9)	1.28(8)	0.84(6)	0.93(7)	1.33(10)	1.61(10)	1.88(11)	1.71(11)
7.08–7.24	1.66(10)	1.96(10)	1.61(9)	1.02(7)	1.16(9)	1.43(10)	1.65(11)	1.97(12)	1.97(13)
7.24–7.41	1.90(11)	2.58(12)	2.42(12)	1.88(10)	1.93(12)	2.04(12)	2.23(12)	2.62(14)	2.86(16)
7.41–7.59	1.78(12)	2.65(14)	3.15(16)	2.64(14)	2.86(15)	2.87(15)	2.87(14)	3.14(16)	3.54(19)
7.59–7.76	1.58(11)	1.95(11)	2.31(13)	2.20(12)	2.73(15)	2.71(14)	2.69(14)	3.03(15)	3.44(18)
7.76–7.94	2.28(12)	2.17(12)	2.24(13)	2.14(12)	3.15(17)	3.37(17)	3.43(17)	3.47(17)	4.12(21)
7.94–8.13	2.83(14)	2.70(13)	2.44(14)	1.94(12)	2.59(15)	3.27(17)	3.53(16)	4.15(18)	5.02(22)
8.13–8.31	3.75(18)	3.94(17)	3.45(17)	2.18(13)	2.35(17)	2.98(18)	4.02(20)	5.42(23)	6.89(30)
8.31–8.51	2.93(16)	2.93(14)	2.42(14)	1.49(10)	1.36(12)	1.53(12)	2.21(14)	3.50(18)	4.43(25)
8.51–8.71	2.76(14)	2.34(12)	1.85(12)	1.12(9)	1.18(10)	1.37(11)	1.90(13)	2.66(15)	3.54(20)
8.71–8.91	2.99(15)	2.45(13)	1.82(12)	1.21(10)	1.41(12)	1.51(11)	1.95(13)	2.64(15)	3.57(20)
8.91–9.12	3.17(16)	2.56(14)	1.84(13)	1.29(11)	1.56(13)	1.94(14)	2.29(14)	2.84(16)	3.69(20)
9.12–9.33	3.28(17)	2.37(14)	1.81(13)	1.44(12)	1.54(14)	1.82(14)	2.28(15)	2.95(16)	3.70(20)
9.33–9.55	3.83(19)	2.84(15)	1.82(13)	1.31(11)	1.45(14)	1.59(13)	2.13(14)	2.87(16)	3.24(18)
9.55–9.77	4.95(23)	3.61(17)	2.24(14)	1.32(11)	1.31(12)	1.42(12)	1.83(14)	2.45(15)	2.71(16)
9.77–10.00	5.55(26)	3.55(17)	2.52(15)	1.56(12)	1.60(14)	1.30(11)	1.54(13)	1.90(14)	2.12(15)
10.00–10.23	4.96(24)	3.80(19)	2.83(17)	1.74(13)	1.81(16)	1.48(13)	1.32(12)	1.73(13)	1.98(15)
10.23–10.47	4.55(24)	3.66(19)	2.54(18)	1.79(14)	1.43(12)	1.45(13)	1.74(14)	2.18(15)	2.32(16)
10.47–10.71	4.65(25)	3.55(20)	2.28(17)	1.53(13)	1.79(15)	1.77(15)	1.90(14)	2.38(15)	2.75(17)
10.71–10.97	5.33(27)	3.83(20)	2.38(17)	1.28(12)	1.54(14)	1.76(14)	1.79(13)	2.24(15)	2.81(18)
10.97–11.22	5.96(31)	4.55(24)	2.55(19)	1.47(14)	1.79(18)	1.71(16)	1.80(14)	2.36(17)	3.12(22)
11.22–11.48	6.13(34)	4.44(25)	2.62(21)	1.76(17)	1.44(16)	1.54(16)	1.73(16)	2.23(18)	3.35(26)
11.48–11.75	6.07(36)	4.55(27)	2.68(22)	1.40(15)	1.69(21)	1.67(19)	1.91(19)	2.26(20)	3.20(26)
11.75–12.02	6.36(39)	4.51(28)	2.59(23)	1.46(18)	1.69(24)	1.69(21)	1.66(18)	2.53(24)	2.92(28)
12.02–12.30	4.53(28)	3.34(22)	1.83(17)	1.03(13)	1.03(14)	1.19(15)	1.40(15)	1.89(17)	2.42(23)
12.30–12.59	4.06(27)	3.20(23)	1.90(19)	1.08(15)	0.92(15)	1.32(18)	1.46(16)	2.05(19)	2.65(23)
12.59–12.88	3.46(24)	2.59(19)	1.54(16)	0.70(11)	0.93(15)	1.06(15)	1.29(14)	1.46(14)	1.82(17)
12.88–13.18	3.91(27)	2.88(21)	1.44(15)	0.76(14)	0.86(14)	1.21(17)	1.15(13)	1.54(15)	2.01(18)
13.18–13.49	3.69(29)	3.00(22)	1.64(20)	0.86(13)	0.88(13)	0.91(13)	1.17(14)	1.41(15)	1.91(18)
13.49–13.80	3.56(29)	2.89(23)	1.63(18)	0.98(16)	0.97(16)	0.84(12)	1.12(15)	1.53(16)	1.84(18)
13.80–14.13	3.25(29)	2.95(24)	1.70(18)	0.86(14)	0.81(13)	0.94(14)	1.26(14)	1.67(17)	1.85(19)
14.13–14.45	3.83(34)	2.91(25)	1.68(20)	0.99(15)	0.68(13)	0.90(14)	1.01(15)	1.74(20)	2.08(23)
14.45–14.79	3.24(29)	2.40(20)	1.41(17)	0.91(17)	0.55(11)	0.66(12)	0.96(15)	1.48(19)	1.81(21)
14.79–15.14	2.97(28)	2.61(22)	2.02(23)	0.80(15)	0.68(13)	0.58(12)	0.73(13)	1.08(16)	1.85(29)
15.14–15.49	2.88(28)	2.34(22)	1.51(21)	0.71(13)	1.05(24)	0.59(13)	0.76(15)	1.17(18)	1.31(18)
15.49–15.85	2.98(31)	2.67(27)	1.46(20)	0.71(13)	0.62(15)	0.85(18)	0.73(15)	0.91(15)	1.09(16)
15.85–16.22	2.35(28)	2.09(21)	1.27(19)	0.67(16)	0.56(15)	0.45(11)	0.52(11)	0.75(14)	0.76(12)
16.22–16.60	2.21(26)	1.90(22)	1.28(20)	0.67(15)	0.62(15)	0.66(17)	0.58(15)	0.76(15)	0.82(16)

TABLE III: The normalized γ angular distributions measured in this work as a function of incident neutron energy, E_α , and laboratory γ -detection angle. The uncertainty on all the laboratory γ -detection angles is $\pm 5^\circ$. The overall scaling of the γ distribution values is arbitrary.

E_α	Laboratory γ -Detection Angle, θ_γ (deg)								
	30	45	60	75	90	105	120	135	150
6.45–6.61	2.67(4)	2.51(4)	2.46(4)	2.30(4)	1.78(3)	1.82(3)	2.16(3)	2.43(4)	2.78(4)
6.61–6.76	2.54(4)	2.32(4)	2.38(4)	2.32(4)	1.81(3)	1.76(3)	2.12(4)	2.26(4)	2.56(4)
6.76–6.92	1.81(3)	1.63(3)	1.59(3)	1.56(3)	1.23(3)	1.19(3)	1.46(3)	1.60(3)	1.74(3)
6.92–7.08	1.83(4)	1.63(3)	1.58(3)	1.48(3)	1.15(3)	1.21(3)	1.44(3)	1.65(3)	1.68(3)
7.08–7.24	1.95(4)	1.74(3)	1.63(3)	1.44(3)	1.03(2)	1.17(3)	1.50(3)	1.76(3)	1.69(3)
7.24–7.41	2.58(4)	2.52(4)	2.24(4)	1.79(3)	1.25(3)	1.50(3)	2.19(4)	2.53(4)	2.33(4)
7.41–7.59	3.34(5)	3.34(5)	3.04(5)	2.30(4)	1.58(3)	1.97(4)	2.86(4)	3.40(5)	3.25(5)
7.59–7.76	3.23(5)	2.97(5)	2.86(4)	2.50(4)	1.80(4)	2.02(4)	2.62(4)	3.05(4)	3.20(5)
7.76–7.94	4.41(7)	3.68(6)	3.59(6)	3.63(6)	3.00(5)	2.99(5)	3.47(6)	3.73(6)	4.21(6)
7.94–8.13	4.47(6)	3.79(5)	3.41(5)	3.29(5)	2.75(5)	2.89(5)	3.54(5)	3.71(5)	4.19(6)
8.13–8.31	4.57(6)	4.07(6)	3.51(5)	3.05(5)	2.43(4)	2.80(5)	3.75(5)	4.05(6)	4.21(6)
8.31–8.51	2.74(4)	2.52(4)	2.20(4)	1.74(3)	1.33(3)	1.63(3)	2.26(4)	2.54(4)	2.43(4)
8.51–8.71	2.67(5)	2.61(4)	2.32(4)	1.74(4)	1.26(3)	1.53(3)	2.19(4)	2.47(4)	2.46(5)
8.71–8.91	2.81(5)	2.80(5)	2.57(5)	1.88(4)	1.32(3)	1.59(4)	2.33(4)	2.59(5)	2.57(5)
8.91–9.12	2.97(6)	2.97(5)	2.79(5)	2.12(4)	1.41(4)	1.69(4)	2.52(5)	2.84(5)	2.78(5)
9.12–9.33	2.99(6)	3.09(5)	2.85(5)	2.21(5)	1.40(4)	1.77(4)	2.59(5)	2.98(5)	2.95(6)
9.33–9.55	2.94(6)	3.14(5)	2.87(5)	2.21(5)	1.45(4)	1.73(4)	2.57(5)	3.01(5)	2.93(6)
9.55–9.77	3.19(6)	3.31(6)	3.08(5)	2.38(5)	1.56(4)	1.74(4)	2.73(5)	3.33(5)	3.15(6)
9.77–10.00	3.32(6)	3.44(6)	3.12(5)	2.38(5)	1.52(4)	1.72(4)	2.75(5)	3.40(6)	3.29(6)
10.00–10.23	3.07(6)	3.22(6)	2.83(5)	2.19(5)	1.46(4)	1.62(4)	2.52(5)	3.03(5)	3.06(6)
10.23–10.47	2.72(5)	2.62(5)	2.34(5)	1.98(4)	1.37(4)	1.47(4)	2.12(4)	2.48(5)	2.66(5)
10.47–10.71	2.73(5)	2.56(5)	2.38(5)	2.00(4)	1.43(4)	1.54(4)	2.15(4)	2.54(5)	2.68(5)
10.71–10.97	3.48(7)	3.38(6)	3.13(6)	2.35(5)	1.66(5)	1.87(5)	2.83(6)	3.37(6)	3.25(6)
10.97–11.22	3.89(8)	3.95(7)	3.54(7)	2.52(6)	1.68(5)	2.11(6)	3.26(7)	3.83(7)	3.57(7)
11.22–11.48	3.92(8)	4.11(8)	3.52(7)	2.45(6)	1.68(6)	2.14(6)	3.36(7)	3.95(8)	3.75(8)
11.48–11.75	2.85(6)	2.95(6)	2.51(6)	1.85(5)	1.33(4)	1.55(5)	2.35(5)	2.80(6)	2.79(6)
11.75–12.02	2.86(7)	2.82(6)	2.52(6)	1.95(5)	1.33(5)	1.54(5)	2.33(6)	2.87(6)	2.65(6)
12.02–12.30	2.72(7)	2.64(6)	2.33(6)	1.82(5)	1.25(4)	1.38(5)	2.19(5)	2.67(6)	2.45(6)
12.30–12.59	2.57(6)	2.45(6)	2.14(6)	1.73(5)	1.25(5)	1.29(4)	1.98(5)	2.28(6)	2.37(6)
12.59–12.88	2.08(6)	1.92(5)	1.77(5)	1.41(4)	1.05(4)	1.09(4)	1.54(4)	1.85(5)	1.83(5)
12.88–13.18	2.55(7)	2.39(6)	2.12(6)	1.77(6)	1.15(5)	1.33(5)	1.89(5)	2.31(6)	2.17(6)
13.18–13.49	2.63(7)	2.47(7)	2.25(6)	1.78(6)	1.15(5)	1.31(5)	1.90(6)	2.24(6)	2.35(7)
13.49–13.80	2.46(7)	2.32(6)	2.17(6)	1.60(5)	1.14(5)	1.30(5)	1.76(6)	2.00(6)	2.16(7)
13.80–14.13	2.47(7)	2.26(6)	2.10(6)	1.61(6)	1.14(5)	1.30(5)	1.75(6)	2.01(6)	2.12(7)
14.13–14.45	2.35(7)	2.18(6)	2.04(6)	1.55(6)	1.10(5)	1.28(5)	1.69(6)	2.07(6)	2.03(6)
14.45–14.79	1.92(6)	1.85(6)	1.70(5)	1.33(5)	0.98(4)	1.16(5)	1.37(5)	1.68(5)	1.60(6)
14.79–15.14	1.98(7)	1.91(6)	1.78(6)	1.40(5)	0.98(5)	1.14(5)	1.41(5)	1.61(5)	1.70(6)
15.14–15.49	1.77(6)	1.66(6)	1.59(5)	1.33(5)	0.92(5)	0.97(5)	1.35(5)	1.45(5)	1.61(6)
15.49–15.85	1.71(6)	1.56(6)	1.52(5)	1.23(5)	0.87(4)	0.85(4)	1.20(5)	1.35(5)	1.55(6)
15.85–16.22	1.62(6)	1.54(6)	1.41(5)	1.09(5)	0.78(4)	0.80(4)	1.15(5)	1.32(5)	1.44(6)
16.22–16.60	1.45(6)	1.43(5)	1.27(5)	1.06(5)	0.78(4)	0.81(4)	1.13(5)	1.28(5)	1.25(5)